To appear in the Astronomical Journal

X-ray Emission from Nitrogen-Type Wolf-Rayet Stars

Stephen L. Skinner

Center for Astrophysics and Space Astronomy (CASA), Univ. of Colorado, Boulder, CO 80309-0389; email: Stephen.Skinner@colorado.edu

Svetozar A. Zhekov[1]

JILA, Univ. of Colorado, Boulder, CO 80309-0440

Manuel Güdel

Institute of Astronomy, ETH Zürich, Wolfgang-Pauli-Str. 27, 8093 Zürich, Switzerland

Werner Schmutz

Physikalisch-Meteorologisches Observatorium Davos and World Radiation Center (PMOD/WRC), Dorfstrasse 33, CH-7260 Davos Dorf, Switzerland

and

Kimberly R. Sokal

Center for Astrophysics and Space Astronomy (CASA), Univ. of Colorado, Boulder, CO 80309-0389

ABSTRACT

We summarize new X-ray detections of four nitrogen-type Wolf-Rayet (WR) stars obtained in a limited survey aimed at establishing the X-ray properties of WN stars across their full range of spectral subtypes. None of the detected stars is so far known to be a close binary. We report *Chandra* detections of WR 2 (WN2), WR 18 (WN4), and WR 134 (WN6), and an *XMM-Newton* detection of WR79a (WN9ha). These observations clearly demonstrate that both WNE and WNL stars are X-ray sources. We also discuss *Chandra* archive detections

[1]On leave from Space Research Institute, Sofia, Bulgaria

of the WN6h stars WR 20b, WR 24, and WR 136 and *ROSAT* non-detections of WR 16 (WN8h) and WR 78 (WN7h). The X-ray spectra of all WN detections show prominent emission lines and an admixture of cool (kT $<$ 1 keV) and hot (kT $>$ 2 keV) plasma. The hotter plasma is not predicted by radiative wind shock models and other as yet unidentified mechanisms are at work. Most stars show X-ray absorption in excess of that expected from visual extinction (A_V), likely due to their strong winds or cold circumstellar gas. Existing data suggest a falloff in X-ray luminosity toward later WN7-9 subtypes, which have higher L_{bol} but slower, denser winds than WN2-6 stars. This provides a clue that wind properties may be a more crucial factor in determining emergent X-ray emission levels than bolometric luminosity.

Subject headings: stars: individual (WR 2; WR 16; WR 18; WR 20b; WR 24; WR 78; WR 79a; WR 134; WR 136) — stars: Wolf-Rayet — X-rays: stars

1. Introduction

X-ray observations of Wolf-Rayet (WR) stars provide an important means of determining physical conditions in their powerful metal-rich winds and in hot wind-blown bubbles which can surround the star. X-ray observations yield information on the temperature, emission measure, and luminosity of hot plasma that can be used to test models of WR X-ray emission, which are largely based on the idea that the X-rays arise in shocked winds. Photoelectric absorption of low-energy X-rays can reveal the presence of gas along the line-of-sight toward the star that is difficult to detect by other means. High-resolution grating spectra can be obtained for the brightest WR X-ray sources and are capable of constraining the location of the X-ray emittng plasma relative to the star, wind parameters, and wind element abundances.

It has been nearly three decades since WR stars were discovered to be X-ray sources by the *Einstein Observatory* (Seward et al. 1979). However, the origin of the X-ray emission is still not totally understood and more than one process may be involved. In the case of single WR stars (and single OB stars), most theoretical work has focused on X-ray production in shocks that are formed in the wind via line-driven instabilities (Lucy & White 1980; Lucy 1982; Owocki, Castor, & Rybicki 1988; Baum et al. 1992; Feldmeier et al. 1997; Gayley & Owocki 1995). Such X-ray emission is expected to be soft (kT $\lesssim$ 1 keV) and X-ray emission lines lines in optically thick winds are predicted to be asymmetric with blueshifted centroids (Owocki & Cohen 2001). Alternate models which attribute shock production to plasmoids moving through the wind have also recently been proposed (Waldron & Cassinelli

2009). The emission of WR binaries is potentially more complex than single stars since it may consist of intrinsic stellar wind-shock emission plus X-rays from a colliding wind shock between the two stars (Prilutskii & Usov 1976; Luo et al. 1990; Stevens, Blondin, & Pollock 1992; Usov 1992). The maximum X-ray temperature of an adiabatic colliding wind shock is proportional to the square of the wind speed perpendicular to the shock front (Luo et al. 1990). Values $kT_{max} \gtrsim 2$ keV are expected for typical WR wind speeds of $v_\infty \sim 1000$ - 5000 km s^{-1}.

Attempts to confirm X-ray wind-shock models observationally have yielded mixed results. Some evidence supporting the colliding wind picture in massive binaries has been obtained from *Chandra* and *XMM-Newton* grating observations of X-ray bright systems such as γ^2 Vel (WC8 + O7.5; Skinner et al. 2001; Schild et al. 2004) and WR 140 (WC7 + O4-5; Pollock et al. 2005). On the other hand, the radiative wind shock picture for single massive stars has not yet found broad observational support. Perhaps the best evidence for X-ray production in radiative wind shocks has come from grating observations of the O4f supergiant ζ Pup, which reveal wind-broadened emission lines (HWHM $\approx$ 600 - 1600 km s^{-1}) with blueshifted centroids (Cassinelli et al. 2001) and a substantial emission measure contribution from low-temperature plasma (Kahn et al. 2001). However, grating spectra of other OB stars show narrower unshifted symmetric emission lines that are more difficult to reconcile with radiative wind shock predictions (e.g. Miller et al. 2002; Schulz et al. 2000; Cohen et al. 2008; Skinner et al. 2008).

Compelling evidence for X-rays from radiative wind shocks in single WR stars is currently lacking. But, very few sensitive pointed observations of single WR stars exist and there are no single WR stars yet known that are bright enough in X-rays to acquire good-quality grating spectra in reasonable exposure times. Even so, CCD observations without gratings are feasible and moderate resolution CCD spectra capable of distinguishing between cool plasma that could arise in radiative wind shocks and hotter plasma due to other processes such as colliding winds can be readily obtained. We have thus initiated an X-ray survey of single WR stars with *Chandra* and *XMM-Newton* aimed at broadening the observational data base and determining their basic properties such as X-ray temperature and luminosity. Our initial targets included both nitrogen-rich WN stars and carbon-rich WC stars. They were selected from the VIIth Catalog of Galactic Wolf-Rayet stars (van der Hucht 2001, herafter vdH01), giving preference to objects lying closest to the Sun with low A_V and no evidence for binarity.

So far, we have observed four apparently single carbon-type WC stars and, surprisingly, none was detected (Skinner et al. 2006; 2009). These are WR 5 (WC6), WR 57 (WC8), WR 90 (WC7), and WR 135 (WC8). The most stringent upper limit is from a *Chandra*

observation of WR 135 for which we obtained log L_X(0.5 - 7 keV) $\leq$ 29.82 ergs s^{-1}. This is $\approx$2 - 3 orders of magnitude below typical X-ray emission levels of WR binaries and X-ray detected WN stars that are not known to be binaries. A non-detection of the WC5 star WR 114 was also reported by Oskinova et al. (2003). Sensitive observations of a broader sample of single WC stars are still needed, but the lack of detections in these exploratory observations already suggests they are either intrinsically faint X-ray emitters, or perhaps X-ray quiet.

In contrast, high-confidence X-ray detections have been obtained for some apparently single WN stars (Skinner et al. 2002a,b; Ignace et al. 2003a; Oskinova 2005; Nazé et al. 2008). These detections are confined primarily to spectral subtypes of WN6 and earlier. Very little is yet known about the X-ray properties of WN7-9 stars. The X-ray luminosities of subtypes WN6 and earlier span a wide range log $L_X \sim$ 31 - 33 ergs s^{-1}. It is remarkable that WN6 stars themselves have L_X values spanning nearly two orders of magnitude. In those cases where good X-ray spectra of early WN subtypes ($\leq$WN6) exist, a multi-temperature plasma is invariably present with a cool component at $kT_1 \lesssim 0.6$ keV and a hotter component at $kT_2 \gtrsim 2$ keV. The cool plasma is compatible with radiative wind shock predictions but the hot plasma is not.

The existence of X-ray emission in late WN7-9 stars has not been thoroughly investigated. But, there are indications that their X-ray luminosity levels are low. An *XMM-Newton* observation of WR 40 (WN8; Gosset et al. 2005) yielded a non-detection with a conservative upper limit log $L_X \leq$ 31.6 ergs s^{-1}. But, an archival *ROSAT* PSPC image (rp200150n00) reveals a marginal detection of the WN9 star WR 79a at a 12.2′ off-axis position, which was our primary motivation for reobserving it at higher sensitivity with *XMM-Newton*.

We report here on sensitive X-ray observations of four WN stars of spectral subtypes WN2 - WN9, namely WR 2 (WN2), WR 18 (WN 4), WR 134 (WN6), and WR 79 (WN9ha). None of these is listed as either a binary or probable binary in the VIIth WR Catalog (vdH01). Periodic line-profile spectroscopic variability in WR 134 at a period P = 2.25 d has been reported by Morel et al. (1999), but no companion has yet been found and other factors such as a rotationally-modulated wind may be responsible for the variability (St.-Louis et al. 2009). All four WN stars were detected (Figs. 1 - 4). We supplement these new detections with selected X-ray archival data for other WN stars, summarize their X-ray properties, and discuss candidate emission mechanisms. Table 1 summarizes the general properties of the WN stars considered in this study.

2. Observations

2.1. *Chandra*

The *Chandra* observations are summarized in Table 2. Exposures were obtained using the ACIS-S (Advanced CCD Imaging Spectrometer) imaging array in faint timed-event mode. A reduced 1/4 subarray size was used for the brighter source WR 134 to minimize any photon pileup. The WR star target was placed at the nominal aimpoint on CCD S3 of the array. The CCD pixel size is 0.492″. Approximately 90% of the encircled energy at 1.49 keV lies within 2″ of the center pixel of an on-axis point source. More information on *Chandra* and its instrumentation can be found in the *Chandra* Proposer's Observatory Guide (POG)[1].

The Level 2 events file provided by the *Chandra* X-ray Center (CXC) was analyzed using standard science threads in CIAO version 4.1.2[2]. The CIAO processing used calibration data from CALDB version 4.1.2. Source detection was carried out using the the CIAO *wavdetect* tool, which correlates the input image with "Mexican Hat" wavelet functions of different scale sizes. We ran *wavdetect* on full-resolution images with a pixel size of 0.″492 using events in the 0.3 - 8 keV range to reduce the background. The *wavdetect* threshold was set at $sigthresh = 1.5 \times 10^{-5}$ and scale sizes of 1, 2, 4, 8, and 16 were used. The *wavdetect* tool provides source centroid positions and net source counts (background subtracted) inside the computed 3σ source region (Table 3).

CIAO *specextract* was used to extract source and background spectra for the WN stars along with source-specific response matrix files (RMFs) and auxiliary response files (ARFs). We used the 3σ source ellipses from *wavdetect* to define the extraction regions and background was extracted from adjacent source-free regions. Background is negligible, contributing <1 count (0.3 - 8 keV) inside the source extraction regions over the duration of each observation. Spectral fitting was undertaken with the HEASOFT *Xanadu*[3] software package including XSPEC vers. 12.4.0. X-ray light curves were extracted using the CIAO tool *dmextract* and checks for source variabilility were carried out on energy-filtered source event files using the Kolmogorov-Smirnov (KS) test (Press et al. 1992) and the Bayesian-method CIAO tool *glvary* (Gregory & Loredo 1992, 1996).

---

[1]See http://asc.harvard.edu/proposer/POG

[2]Further information on *Chandra* Interactive Analysis of Observations (CIAO) software can be found at http://asc.harvard.edu/ciao.

[3]http://heasarc.gsfc.nasa.gov/docs/xanadu/xanadu.html.

2.2. *XMM-Newton*

Table 2 summarizes the *XMM-Newton* observation of WR 79a. Data were acquired with the European Photon Imaging Camera (EPIC), which provides charge-coupled device (CCD) imaging spectroscopy from the pn camera (Strüder et al. 2001) and two nearly identical MOS cameras (MOS1 and MOS2; Turner et al. 2001). The observation was obtained in full-window mode using the thick optical blocking filter. The EPIC cameras provide energy coverage in the range E ≈ 0.2 - 15 keV with energy resolution E/ΔE ≈ 20 - 50. The MOS cameras provide the best on-axis angular resolution with FWHM ≈ 4.3″ at 1.5 keV.

Data were reduced using the *XMM-Newton* Science Analysis System (SAS vers. 7.1) using the latest calibration data. Event files based on pipeline processing carried out at the *XMM-Newton* Science Operations Center were filtered to select good event patterns. Further filtering based on event energies was done to reduce background emission. No time filtering was required.

Spectra and light curves were extracted from circular regions of radius $R_e = 15''$ centered on WR79a, corresponding to ≈68% encircled energy at 1.5 keV. This approach reduces the number of background counts while capturing most of the source counts. Total source counts (Table 3) were measured in a larger circular region of radius r = 45″ corresponding to ≈90% encircled energy at 1.5 keV. Background spectra and light curves were obtained from circular source-free regions near the source. The SAS tasks *rmfgen* and *arfgen* were used to generate source-specific RMFs and ARFs for spectral analysis. The data were analyzed using the HEASOFT *Xanadu* software package

2.3. Archival Data

We have examined *Chandra* and *ROSAT* archive data for selected WN stars which are not known to be binaries. Our archive analysis is not exhaustive and was restricted to a few high-interest objects for which either good CCD spectra or useful upper limits were obtained. Analysis of *Chandra* archive data was carried out using the same procedures described above (Sec. 2.1). *ROSAT* images were analyzed using the *Ximage* image analysis tool, which is part of the HEASOFT *Xanadu* package. Results of the archive analysis are summarized in Section 3.3 and in Tables 3 and 5.

3. Results

3.1. General X-ray Properties

Table 3 summarizes the X-ray properties of the four newly-detected WN stars and three WN stars from the *Chandra* archive (WR 20b, WR 24, and WR 136). There is very good agreement between the X-ray positions and the optical positions of the WN stars given in the *HST* Guide Star Catalog (GSC). Radial offsets between the X-ray and optical positions are $\leq 0.3''$ for the new detections, being within the 1σ range of *Chandra* [4] and *XMM* [5] positional accuracy. Similar offsets were obtained for the archive detections. There is thus no reason to doubt that the X-ray sources are the optically-identified WR stars.

No significant X-ray variability was detected in any of the targets, but sampling in the time domain spans less than $\approx$10 hours for the four new detections and $\lesssim 1$ day for the archive sources. Thus, variability on longer timescales exceeding one day cannot yet be ruled out.

The X-ray spectra of the four new detections are shown in Figure 5 and the archive spectra in Figure 6. All spectra show some absorption below $\approx$0.8 keV as well as prominent emission lines or line complexes indicative of thermal emission. The most prominent lines are the unresolved Mg XI He-like triplet at 1.33 - 1.35 keV (maximum line power temperature log T_{max} = 6.8 K) and the unresolved Si XIII triplet at 1.84 - 1.86 keV (log T_{max} = 7.0 K). The higher temperature S XV line at 2.46 keV (log T_{max} = 7.2 K) is also seen in all stars, but is very faint in WR 2. The high-temperature line from He-like Ar XVII (log T_{max} = 7.3 K), is detected in several stars and is quite strong in WR 20b. Faint emission near 3.9 keV in the WN6h stars WR 20b and WR 136 may be due to He-like Ca XIX (log T_{max} = 7.5 K) but we classify this line only as a possible detection. The Fe Kα complex (Fe XXV; 6.67 keV log T_{max} = 7.6 K) is detected in WR 20b, WR 134, and WR 136. This line is a signature of very hot plasma, which is undoubtedly present in these latter three WN6h stars.

3.2. X-ray Spectral Fits

We have attempted to fit the spectra with various emission models, including the XSPEC variable-abundance optically thin plasma model *vapec* (Smith et al. 2001) and the constant temperature plane-parallel shock model *vpshock* (Borkowski et al. 2001, and references

[4] http://asc.harvard.edu/proposer/POG

[5] http://xmm2.esac.esa.int/docs/documents/CAL-TN-0018.pdf

therein). All models included a photoelectric absorption component (XSPEC model *wabs*) which was used to determine the equivalent neutral H column density N_H.

Element abundances are expected to deviate strongly from solar composition in WN stars as the result of advanced nucleosynthesis. H is depleted along with C and O, while He and N are enriched (van der Hucht et al. 1986; hereafter VCW86). Because of the moderate CCD spectral resolution of ACIS-S and EPIC and limited total source counts, we are not able to place tight constraints on element abundances using the X-ray spectra. We have thus adopted the generic WN abundances of VCW86 (Table 4) as starting values in spectral fits using the *vapec* and *vpshock* models. Selected elements were allowed to deviate from the VCW86 values to improve the fits, as detailed in Tables 4 and 5. The total X-ray absorption likely includes contributions from solar abundance material in the interstellar medium and stellar wind absorption from material enriched with heavy elements. The CCD spectra do not provide sufficient information to disentangle solar and nonsolar absorption, and we have thus modeled X-ray absorption using solar abundances (XSPEC *wabs*; Anders & Ebihara 1982).

Our main spectral analysis results can be summarized as follows: (i) single-temperature optically-thin plasma models (1T *vapec*) do not provide acceptable fits, even if abundances are allowed to vary, (ii) two-temperature models (2T *vapec*) are acceptable but the goodness-of-fit statistic (χ^2) is sensitive to abundances; (iii) all stars show both a cool ($kT_1 < 1$ keV) and hot ($kT > 2$ keV) plasma component, (iv) most stars show X-ray absorption in excess of that expected from their optical extinction A_V, (v) fits using isothermal plane-parallel shock models are not as good as 2T *vapec* (WR 20b excepted).

3.2.1. Optically Thin Plasma Models (vapec)

In all cases, the 2T model requires a cool component at $kT_1 \approx 0.3$ - 0.6 keV plus a hotter component at $kT_2 > 2$ keV. The best-fit value of kT_2 for WR 2 is sensitive to the S abundance, which is not well-constrained by the data. We thus quote only a lower 90% confidence bound on kT_2 for WR 2. The respective normalization values (*norm*) for each component show that most of the emission measure in WR 2, WR 18, and WR 79a is associated with the cooler component, while the hotter component clearly dominates in WR 134 and WR 136.

The best-fit neutral-H absorption column density (N_H) is a factor of ≈2 - 4 lower in WR 2 than in the other three stars. Using the conversion $N_H = 2.22 \times 10^{21}\ A_V\ cm^{-2}$ (Gorenstein 1975), it is apparent from Table 4 that the X-ray derived N_H is consistent with that expected

from A_V = 1.58 mag for WR 2 (Table 1). However, the N_H for WR 18, WR79a, and WR 134 is a factor of ∼2 - 4 greater than anticipated from A_V, implying the presence of X-ray absorbing gas (e.g. the wind) that does not contribute significantly to the optical extinction. Excess absorption is also present in the archive detection WR 20b.

Some improvement in the 2T *vapec* fits was obtained by allowing elements with detectable line emission (N, Ne, Mg, Si, S, Fe) to deviate from the generic WN values (Table 4 and 5 notes). In particular, our fits of several stars were improved by using S abundances larger than the value given in VCW86 (which was based on cosmic mass fraction).

3.2.2. Plane-Parallel Shock Models (vpshock)

Given the expectation that WR star X-ray emission may arise in shocked winds, we attempted to fit the spectra of all detections except WR 18 with *vpshock* in order to determine if a simplistic constant-temperature shock model could reproduce the spectra. There are insufficient counts in WR 18 to establish a clear preference between thin plasma models and shock models. The *vpshock* fits used data from the Atomic Plasma Emission Database (APED) [6] to calculate the spectrum (XSPEC option *neivers* 2.0).

For the new detections, reasonably good *vpshock* fits were obtained for both WR 2 and WR 134, but we do not find a clear preference for *vpshock* over the 2T *vapec* model in either case. For WR 2, *vpshock* gives shock temperatures in the range $kT_{shock} \approx$ 1.5 - 3.5 keV, but in order to obtain acceptable fits the abundances of elements with line emission above 2 keV (most notably S and Ar) must be increased to very high values. When abundances are fixed at the generic WN values, *vpshock* underestimates the hard flux above 2 keV. When abundances are allowed to vary, the model attempts to correct for this flux deficit by running up the S and Ar abundances while at the same time keeping $kT_{shock} \approx 2$ keV. This is likely a consequence of attempting to fit a multi-temperature plasma with an overly simplistic constant-temperature shock model. For WR 134, high shock temperatures $kT_{shock} \geq 10$ keV are required and even with such high temperatures the χ^2 fit statistic is not as good as obtained with 2T *vpaec*.

For the archive detections, the *vpshock* fits for WR 24 and WR 136 are reasonably good above 1 keV but the shock model underestimates the observed flux of the softer emission below ≈1 keV. WR 20b provides an interesting exception because the *vpshock* model actually provides a better fit to its spectrum than 2T *vapec* (Table 5 notes). The inferred shock

[6] http://cxc.harvard.edu/atomdb/sources_aped.html

temperature kT_{shock} = 3.9 keV is quite high. However, the soft emission below 1 keV that cannot be accurately reproduced with *vpshock* in the other stars is not detected in WR 20b (Fig. 6). Thus, the good results obtained with *vpshock* for WR 20b may simply be a consequence of its higher absorption.

3.3. Comments on Specific Stars

WR 2 (WN2): WR 2 is a new *Chandra* detection and is the earliest WN subtype in our sample. The V = 12.73 mag object (*HST* GSC J010522.98+602505.1) lying 13.9″ south of WR 2 was not detected by *Chandra*. WR 2 lies in a neutral hydrogen void (Arnal et al. 1999). No significant spectroscopic variability was found for WR 2 in the recent study of St.-Louis et al. (2009). However, unusual round-shaped emission line profiles have been reported for WR 2 that were interpreted as signaling rapid rotation near breakup (Hamann et al. 2006).

As Table 3 shows, it is the softest X-ray source of the detected WN stars as judged by its median photon energy E_{50} = 1.04 keV. Spectral analysis confirms that the X-ray absorption toward WR 2 is less than the other three stars, resulting in the detection of more soft photons below 0.7 keV and a lower median photon energy. Events were detected in WR 2 down to energies of ≈0.3 keV as well emission at higher energies up to ≈3 keV.

The *Chandra* spectrum is interesting because it shows an emission feature near 0.5 keV that likely includes a contribution from the low-temperature hydrogen-like N VII Ly α line (log T_{max} = 6.3 K). The intermediate temperature Ne X line at 1.02 keV (log T_{max} = 6.7 K) is also detected, as well as faint emission from the higher-temperature Si XIII and S XV lines. Thus, cool and hot plasma features are present in the same star. Two issues related to 2T *vapec* fits are worthy of note. This model is able to reproduce most of the broad emission feature near 0.5 keV with the N VII Lyα line (E_{lab} = 500.3 eV). But, there is some residual at slightly higher energies of 530 - 540 eV that is not reproduced by this line. The O VII resonance line is not obviously detected and in any case it lies at a higher energy (574 eV) and cannot account for this residual. However, other ions with lab energies slightly above that of N VII could be contributing to the residual including N VI (532.6 eV), S XIV (538.9 eV), and Ca XVI (546.8 eV). The 2T *vapec* model also has difficulty reproducing all of the flux in the faint feature near 2.46 keV (S XV) unless a very high S abundance is assumed.

WR 16 (WN8h): This star is of interest because of its later WN8h subtype and moderate extinction A_V = 1.8 mag (vdH01). WR 16 was not detected in *ROSAT* PSPC image rp200715n00, which has an exposure livetime of 7,465 s. Our analysis of the PSPC data

gives a 3σ upper limit on the total band count rate $\leq$1.8 c ksec^{-1}. The PSPC is sensitive at lower energies of $\approx$0.15 - 2.5 keV. This equates to a conservative 3σ upper limit log L_X(0.3 - 8 keV) $\leq$ 31.7 ergs s^{-1}, assuming a distance d = 2.37 kpc (vdH01). The conversion from PSPC rate to unabsorbed flux and L_X was carried out using the Portable Interactive Multi-Mission Simulator (PIMMS)[7] assuming $N_H = 4 \times 10^{21}$ cm^{-2} corresponding to $A_V = 1.8$ mag (Gorenstein 1975) and a Raymond-Smith thermal plasma model with emission measure equally distributed between a cool component at $kT_1 = 0.6$ keV and a hotter component at $kT_2 = 3.0$ keV.

WR 18 (WN4): This WN4 star is associated with the asymmetric nebula NGC 3199, which has been modeled as a wind-blown bubble by Dyson & Ghanbari (1989). Cold circumstellar molecular gas has been reported by Marston (2001, 2003). It is a new *Chandra* detection and its spectrum shows a prominent Si XIII line and the hotter S XV line.

WR 20b (WN6h): This star was detected as a bright source in a previous *Chandra* observation of the massive stellar cluster Westerlund 2 (ObsId 6411; Nazé et al. 2008). Its X-ray emission is heavily-absorbed and exceptionally hard with a median photon energy $E_{50} = 3.04$ keV. We were unable to obtain acceptable fits with a 1T *vapec* model but a 2T *vapec* model is satisfactory and requires a hot plasma component at $kT_2 \approx 4$ - 5 keV. The isothermal plane-parallel shock model *vpshock* provides a slightly better fit with an inferred shock temperature $kT_{shock} = 3.9$ keV. The X-ray absorption is greater than for any other WN star in our sample. The absorption determined from both *vapec* and *vpshock* models yields a ratio of X-ray to optically-determined absorption $N_H/N_{H,vis} \approx 3$. The ACIS-I spectrum shows high-temperature emission lines including Ar XVII (3.13 keV) and Fe XXV (6.67 keV). The distance to WR 20b is quite uncertain. Values range from d = 2.27 kpc (vdH01) up to 8 kpc (Nazé et al. 2008). Even at the low end of this range, its X-ray luminosity is very high for a WN star (log $L_X > 33.5$ ergs s^{-1}). Its high L_X and hard spectrum are reminiscent of colliding wind binaries, suggesting that this object may not be a single star (Sec. 4.6).

WR 24 (WN6ha): This star was detected as a bright off-axis X-ray source in an archival *Chandra* guaranteed time observation (GTO) of the Carina region (GTO ObsId 9482). Its ACIS-I spectrum shows a remarkably strong S XV emission line at 2.46 keV, as well as the high-temperature Ar XVII (3.13 keV) line and possible faint Fe line emission in the 6.4 - 6.7 keV range. A 2T *vapec* model provides a satisfactory fit with a hot plasma component at $kT_2 \approx 4$ keV. The absorption $N_H = 0.76$ [0.44 - 1.05] $\times 10^{22}$ cm^{-2} is several times larger than would be expected from $A_V = 0.56$ mag (vdH01). At an assumed distance d = 3.24 kpc (vdH01), a high unabsorbed X-ray luminosity log $L_X = 33.0$ ergs s^{-1} is inferred, only slightly

[7]http://heasarc.nasa.gov/docs/software/tools/pimms.html

less than for WR 20b. Because of its high L_X and high L_{bol}, WR 24 is another candidate unresolved binary system (Sec. 4.6).

WR 78 (WN7h): This WNL star is similar to WR 16, having moderate extinction A_V = 1.5 mag and is relatively nearby at d = 1.99 kpc (vdH01). A previous tabulation of WN star X-ray observations by Oskinova (2005) listed WR 78 as a *ROSAT* PSPC detection. Our analysis of archival *ROSAT* PSPC images rp200716n00 does not confirm this. We report a non-detection in the total band and soft band images. Weak signal may be present in the hard band PSPC image, but the signal-to-noise ratio S/N $\approx$ 2 is not sufficient to classify it as a detection. We obtain a 3σ upper limit on the total band PSPC count rate $\leq$2.97 c ksec^{-1} based on an exposure livetime of 10,121 s. The corresponding 3σ luminosity upper limit from PIMMS is log L_X(0.3 - 8 keV) $\leq$ 31.7 ergs s^{-1} (at d = 1.99 kpc). This assumes N_H = 3.3 $\times$ 10^{21} cm^{-2} corresponding to A_V = 1.5 mag (Gorenstein 1975) and a 2T Raymond-Smith thermal plasma model as for WR 16 above.

WR 79a (WN9ha): This is a new and important *XMM-Newton* detection, being the latest WN subtype in our sample and the first unambiguous X-ray detection of a WNL star in the WN7-9 range. There is a fainter near-IR source (2MASS J165458.09−410903.6) at an offset of 4.″8 from WR 79a (see also Mason et al. 1998), but the X-ray positional accuracy is capable of distinguishing between this object and WR 79a. Radio continuum emission has been detected (Bieging, Abbott, & Churchwell 1989) and follow-up observations suggest a nonthermal radio component may be present (Cappa, Goss, & van der Hucht 2004). WR 79a (= HD 152408) was formerly classified as O8:Iafpe but was subsequently reclassified as WN9ha based on the analysis of its optical, UV, and IR spectra by Crowther & Bohannan (1997). Its EPIC spectrum reveals a strong Si XIII line and higher temperature S XV and Ar XVII lines. Since this star resembles an O8 supergiant, we have considered solar abundance spectral fits as well as the fit based on WN abundances given in Table 4. The solar abundance fit gives comparable temperatures to the WN abundance fit but yields a slightly higher N_H and L_X (Table 4 Notes). Regardless of the reference abundances used, the L_X of WR 79a is at the low end of the range found here for WN stars.

WR 134 (WN6h): This is a new *Chandra* detection and a luminous X-ray source with a very hot component. It is surrounded by a ring nebula (Chu et al. 1983; Miller & Chu 1993). Because of its unusual 2.25 d periodic spectroscopic variability, it has been the subject of numerous previous studies (e.g. Howarth & Schmutz 1992; Schulte-Ladbeck et al. 1992; Morel et al. 1999; St.-Louis et al. 2009). The possibility that the 2.25 d periodicity might be due to a compact companion has been debated but there are difficulties with this interpretation (Morel et al. 1999). We discuss the compact companion hypothesis further in Section 4.4.

WR 136 (WN6h): WR 136 is surrounded by the ring nebula NGC 6888 (Gruendl et al. 2000) which is a source of diffuse X-ray emission (Bochkarev 1988; Gruendl, Guerrero, & Chu 2003; Chu, Gruendl, & Guerrero 2006). The WR star was detected at ≈8′ off-axis in a deep 93 ksec *Chandra* exposure of NGC 6888 (ObsId 3763). The ACIS-S spectrum is faint, but quite remarkable. The spectrum is dominated almost entirely by emission lines, including the high-temperature S XV line (2.46 keV), possible faint emission from Ca XIX (3.9 keV), and a feature near 6.67 keV that is likely Fe XXV. Attempts to fit the spectrum with a 2T *vapec* model using a single absorption component were unstable and resulted in high runaway temperatures for the hot component. A modified 2T *vapec* model that allows for different absorptions toward the cool and hot component is stable and provides a good fit (Table 5). The absorption derived for the cool component is consistent with that expected for previous extinction estimates $A_V = 1.73 \pm 0.32$ mag (vdH01). However, the best-fit absorption of the hot component is a factor of ≈8 larger. The physical picture that emerges from such a model is that the cool X-ray emission originates far from the star and incurs little or no wind absorption. In contrast, the hot component originates deep within the wind and much closer to the star and is subject to strong attenuation by the wind. The inferred X-ray luminosity is sensitive to the temperature of the cool component but most fits yield values of log L_X(0.3 - 8 keV) ≈ 31.5 ergs s^{-1}, assuming the *Hipparcos* distance d = 1.64 kpc. Thus, WR 136 seems to be of lower X-ray luminosity than other WN6 stars in the sample.

4. Discussion

The new observational results discussed above provide the most detailed picture to date of the X-ray emission of apparently single WN stars. We comment below on specific aspects of their X-ray emission and possible emission processes.

4.1. X-ray Absorption

The visual extinction A_V for the WN stars in our sample is dominated by interstellar material along the line-of-sight. There is insufficient dust in the winds of WN stars to significantly affect A_V, in contrast to some WC stars whose dusty winds can absorb and re-radiate stellar light (van der Hucht, Williams, & Thé 1987). The A_V values in Table 1 can be used to calculate an equivalent neutral H absorption column density along the line-of-sight using the conversion $N_{H,vis} = 2.22 \times 10^{21} A_V$ cm^{-2} (Gorenstein 1975). Assuming that the winds of WN stars have a negligible effect on A_V, the resulting value of $N_{H,vis}$ is a measure of interstellar absorption. In Tables 4 and 5 we give the ratio of the X-ray to

optically-derived absorption column densities $N_H/N_{H,vis}$. This ratio is greater than unity for all WN stars except WR 2. That is, the X-ray absorption is greater than expected based on visual extinction estimates. The largest absorption excesses are found for WR 20b and WR 134. For the double-absorption model of WR 136, there is no significant absorption excess for the cool component but a large excess is found for the heavily-absorbed hot component.

Most of the excess X-ray absorption likely occurs in the metal-rich WR wind, but in some cases cold circumstellar molecular gas may also contribute. It may not be a coincidence that WR 2 has little or no excess absorption given that it has the highest effective temperature of the four newly-detected stars ($T_* = 141$ kK, Hamann et al. 2006) and the lowest wind density parameter $\dot{M}/v_\infty$. Higher temperatures (along with higher ionization) plus lower densities would increase wind transparency to X-rays.

If the X-rays are formed in the wind then some wind absorption is expected, especially for lower energy photons. For an ideal spherical wind, the radius of optical depth unity $R_{\tau=1}$ beyond which X-ray photons can escape (the "exospheric approximation") depends on several factors including photon energy, mass-loss parameters, photoelectric absorption cross-sections, and wind abundances (e.g. Owocki & Cohen 1999). In Figure 7, we plot $R_{\tau=1}$ as a function of photon energy for the four new detections. We have assumed an ideal spherical, homogeneous, constant-velocity wind with the mass-loss parameters as given in Table 1, canonical WN abundances (VCWH86), and the photoelectric absorption cross-sections of Balucińska-Church & McCammon (1992, hereafter BM92). It is apparent that under the above assumptions, soft photons with $E < 1$ keV emerge at large distances from the star $R_{\tau=1} \gtrsim 1000\ R_\odot$. Taking WR 134 as a specific example, the softest photons visible in its spectrum (Fig. 5) at $E \approx 600$ eV have $R_{\tau=1}(600\ \mathrm{eV}) = 9262\ R_\odot \approx 1750\ R_*$, assuming $R_* = 5.29\ R_\odot$ (Hamann et al. 2006).

The above estimates, which are based on the assumption that the wind is homogeneous and spherically symmetric, suggest that the softest X-ray photons detected in the WN star spectra emerge at large distances of thousands of stellar radii or more from the star. These are only rough estimates because wind abundances and mass-loss parameters are poorly-known. Furthermore, there is accumulating evidence that the winds of WR stars are clumped rather than homogeneous (Moffat et al. 1988; Robert 1994; Lépine et al. 2000), in which case the X-rays could escape from smaller radii closer to the star. Even if the wind is the dominant absorber, other factors such as cold dense circumstellar gas could also contribute. Such gas has been detected around WR 18 and may be a vestige of mass-loss in previous evolutionary phases (Marston 2001; 2003).

4.2. Wind Shocks

The radiative wind shock picture cannot explain the high-temperature plasma seen in the X-ray spectra of WN stars, but the temperature of the cooler plasma $kT_1 \approx 0.3$ - 0.6 keV is compatible with radiative wind shocks. Of the four stars observed, WR 2 shows the coolest emission. Assuming its cool plasma originates in wind shocks, we equate the best-fit temperature of the cool component with the shock temperature, that is $kT_1 = 0.32$ [0.24 - 0.45] keV = kT_s. For an adiabatic shock the maximum shock temperature is $kT_s = (3/16)\bar{m}v_s^2$, where v_s is the shock velocity perpendicular to the shock front (Luo et al. 1990). For a helium-rich WN wind $\bar{m} = (4/3)m_p$ where m_p is the proton mass. An equivalent form of this relation that is easier to apply is $kT_s = 2.61[v_s/1000 \text{ km s}^{-1}]^2$ keV.

The inferred shock speed for WR 2 is then $v_s = 350$ [304 - 416, 90% confidence range] km s^{-1}. This value is plausible, being only about one-fifth the terminal wind speed (Table 1) and within the range of shock velocity jumps found in numerical simulations of radiatively driven winds in O-type stars (Owocki et al. 1988; Feldmeier et al. 1997). The slightly higher values $kT_1 \approx 0.6$ keV for the other three stars give shock speeds $v_s \approx 480$ km s^{-1}.

The unabsorbed flux of the cool X-ray component in WR 2 (Table 4) gives a cool-component luminosity $\log L_{X,1} = 32.47$ (ergs s^{-1}) and $\log [L_{X,1}/L_{wind}] = -4.94$. So there is sufficient wind kinetic energy to power the soft X-ray emission even at a rather low conversion efficiency from kinetic to radiative energy. But, numerical models show that forward shocks decay with radius (Feldmeier et al. 1997) and it remains to be demonstrated by detailed simulations that X-ray emitting wind shocks can persist as coherent structures in WR winds out to large distances of hundreds to thousands of stellar radii (Sec. 4.1).

We now consider another star, WR 20b, which is an interesting case because of the good fit obtained with an isothermal plane-parallel shock model. The best-fit shock temperature $kT_s = 3.86$ [2.97 - 6.53] keV is too high to explain by radiative wind shocks, but is plausible for colliding wind shocks. If the wind of WR 20b is shocking onto an unseen companion, then the inferred shock velocity perpendicular to the interface is $v_s = 1216$ [1067 - 1582] km s^{-1}. This estimate is for an adiabatic shock and assumes a pure He wind for the WN star. The above value is reasonable, being comparable to the terminal wind speeds of WN6 stars (Crowther 2007; Hamann et al. 2006).

4.3. Magnetically-Confined Winds

There are at present no detections of magnetic fields in WR stars to our knowledge. But, if magnetic fields of sufficient strength exist then they could confine the ionized wind

into two oppositely directed streams which collide near the magnetic equator and form a magnetically-confined wind shock (MCWS). This mechanism is of interest because it is capable of producing hot X-ray plasma over a range of temperatures up to several keV (Babel & Montmerle 1997) and could potentially explain the hotter plasma seen in the WN star spectra.

A rough estimate of the field strength needed to confine the wind can be obtained using the confinement parameter $\eta = B_{eq}^2 R_*^2 / \dot{M} v_\infty$ where B_{eq} is the field strength at the magnetic equator (ud-Doula & Owocki 2002). For $\eta \approx 1$ the wind is marginally-confined by the B-field, for $\eta << 1$ the wind overpowers the field and is not confined, and for $\eta >> 1$ the wind is strongly-confined. Assuming $\eta \approx 1$ (marginal confinement) and adopting the mass-loss parameters and stellar radii in Table 1, one obtains magnetic field strengths in the range B_{eq} $\approx$ 3.5 kG (WR 134) up to 17 kG (WR 2). These fields are for marginal confinement and larger fields would be needed for strong confinement. Without concrete evidence for strong B fields in WR stars, this mechanism must be considered speculative.

4.4. Close Binary Companions

Our four new detections and archive sources were selected on the basis that they are so far not known to be close (spectroscopic) binary systems. Thus, any attempt to explain their X-ray emission by invoking an unseen companion is not strongly motivated on observational grounds. However, it is worth keeping in mind that close companions at sub-arcsecond spacings are difficult to detect, especially when in low-inclination orbits.

Of the WN stars in our sample, WR 134 has been regarded as a possible close binary system because of its known 2.25 day periodic line profile changes. This issue has been previously discussed by Morel et al. (1999). However, binarity has not yet been demonstrated and a rotationally-modulated wind is an alternative explanation for the variability (St.-Louis et al. 2009). A close companion, if present, could potentially explain the hard X-ray emission in WR 134. Hard X-rays could be produced by the WR wind accreting onto a compact object or by the wind shocking onto the surface of a normal (nondegenerate) stellar companion. But this interpretation encounters some difficulties.

The most compelling example known so far of a WR star accreting onto a compact object is Cyg X-3. It has a high X-ray luminosity $L_X \sim 10^{38}$ ergs s^{-1} and the companion is thought to be either a black hole or a neutron star (van den Heuvel & De Loore 1973; Schmutz, Geballe, & Schild 1996; Lommen et al. 2005). If the putative companion of WR 134 were a neutron star, then the predicted X-ray luminosity from wind accretion is log $L_{X,acc}$

$\sim 10^{37}$ ergs s^{-1} (Morel et al. 1999). This exceeds the observed value for WR 134 (Table 4) by more than four orders of magnitude. This interpretation is thus untenable unless some mechanism is operating to inhibit wind accretion (see Davidson & Ostriker 1973 or Lipunov 1982 for details on such mechanisms). A similar luminosity mismatch has also been noted for the WN star WR 6 (EZ CMa) by Skinner et al. (2002b). It also undergoes periodic optical variability (P = 3.76 d; Firmani et al. 1980) of unknown origin and a neutron star companion has been suggested as a possible explanation. In the case of WR 134, there are other obstacles to overcome if the putative companion is a neutron star of typical mass M_{ns} $\approx$ 1.4 $M_\odot$. If P = 2.25 d is interpreted as an orbital period, then Kepler's third law gives a separation $a \approx 20\ R_\odot \approx 4\ R_*$. Here we have adopted $M_{WR} = 19\ M_\odot$ and radius $R_* = 5.3\ R_\odot$ for WR 134 (Hamann et al. 2006). Unless the wind is inhomogenous, X-rays at energies E $\approx$ 2 - 3 keV (obviously present in the spectrum) could not escape from such small radii. Specifically, if we use the mass-loss parameters for WR 134 in Table 1 and canonical WN abundances (VCW86), then $R_{\tau=1}$(2 keV) $\approx$ 89 R_*. The slightly different mass-loss parameters for WN6 stars in Crowther (2007) give $R_{\tau=1}$(2 keV) $\approx$ 36 R_*.

Given the luminosity mismatch obtained in the neutron star companion model, it seems more likely that any unseen companion is a normal (nondegenerate) star. It would have been difficult for a massive companion ($M_{comp} \approx M_{WR}$) to have escaped detection, but a lower mass star ($M_{comp} << M_{WR}$) would be more difficult to detect. The possibility of a low-mass companion was previously considered in our analysis of the similar WN-type star WR 6 (Skinner et al. 2002b). Likewise, for WR 134 it can be shown that the hard-component X-ray luminosity could be accounted for by the WR wind impacting the surface of a lower-mass star of subsolar radius (Usov 1992). Furthermore, the plasma temperature of the hot component of WR 134 is compatible with maximum values expected from a shocked wind at or near the terminal wind speed of WR 134. Specifically, $v_\infty \approx$ 1700 - 1960 km s^{-1} (St.-Louis et al. 2009) gives $kT_s \approx$ 7.5 - 10. keV. However, such a low-mass companion would be located very close to WR 134 if P = 2.25 d is the orbital period. Separations of $<5\ R_*$(WR) are inferred from Kepler's third law, so again the escape of X-rays through the wind is potentially problematic. This problem is mitigated if the wind is clumped or if an unseen companion is present at a larger separation than inferred above, resulting in a lower WR wind density at or near the companion surface.

4.5. Emerging Trends in WN Star X-ray Emission

The sample of single WN stars for which X-ray parameters have been reliably determined from good-quality CCD spectra is not yet large enough to establish any clear correlations

between stellar and X-ray properties. Other factors such as uncertain distances, bolometric luminosities, and mass-loss parameters hinder correlation studies and can mask dependencies.

However, X-ray observations now span the full range of spectral subtypes from WN2 to WN9 and a few notable trends are beginning to emerge. As Figure 8 shows, there is an apparent falloff in L_X toward later WN7-9 subtypes. The WN9ha star WR 79a has the lowest L_X of any detected single WN star so far. And, the WN8h star WR 40 was undetected in a previous *XMM-Newton* observation at an upper limit log $L_X < 31.6$ ergs s^{-1} (Gosset et al. 2005). This upper limit is a factor of 3.5 below the L_X determined from the detection of WR 79a. Figure 8 also includes upper limits for WR 16 (WN8h) and WR 78 (WN7h) based on short-exposure *ROSAT* PSPC archive images. Since *ROSAT* was not sensitive to hotter plasma above ≈2.5 keV, which is likely present, the PSPC upper limits should be considered tentative until observations spanning a broader X-ray bandpass can be obtained.

The apparent decrease in L_X for WN7-9 subtypes is surprising because it is in the opposite sense of L_{bol}, which is larger for WN7-9 stars than WN2-6 stars (Table 1; Hamann et al. 2006; Crowther 2007). We plot L_X versus L_{bol} in Figure 9. This figure clearly illustrates that even though the WN and WC stars observed to date have similar L_{bol}, the WC stars (all undetected) are at least 1 - 2 orders of magnitude less luminous in X-rays. Considering only the detected WN stars, one might be tempted to argue for a weak increase in L_X with L_{bol}. But, the absence of X-ray detections for three WNL stars with high L_{bol} (WR 16, 40, 78) is clearly at odds with this picture. This result is contrary to the trend seen in OB stars, for which L_X generally increases with L_{bol}, albeit with large scatter (Berghöffer et al. 1997). Thus, some other stellar parameters besides L_{bol} are critical for determining X-ray luminosity levels in these WN stars, and wind properties may play a key role.

The classical theory of hot star winds in the exospheric approximation predicts that $L_X \propto (\dot{M}/v_\infty)^{1+s}$ where s = 1 for optically thin winds and $-1 < s < 0$ for optically thick winds (Owocki & Cohen 1999). The existing WN star data do not show any clear increase in L_X with $\dot{M}/v_\infty$. On the contrary, WR 79a is the least luminous X-ray source amongst the new detections, but has the largest $\dot{M}/v_\infty$.

From the standpoint of observations, an increase in L_X with wind kinetic energy would seem to be more promising. In Figure 10, we plot L_X versus $L_{wind} = (1/2)\dot{M}v_\infty^2$ for several WN stars for which good X-ray CCD spectra are available. Despite uncertainties in $\dot{M}$, v_∞, and distances, there is a noticeable increase in L_X toward higher values of L_{wind} for the stars considered in this study.

A notable outlier is WR 136, which is underluminous in X-rays by at least a factor of ∼5 compared to the other WN6 stars (Fig. 8) and also has a low L_X for its wind luminosity

(Fig. 10). We have assumed d = 1.64 kpc for WR 136 based on its *Hipparcos* parallax. Other distance estimates are less (e.g. d = 1.26 kpc, vdH01), so a distance underestimate is not likely to be responsbile for its lower L_X. One way to correct for the low L_X is to postulate very cool undetected plasma (kT < 0.2 keV) that is masked by absorption. If such plasma is present, then values log $L_X > 32.0$ ergs s^{-1} are possible.

Equally interesting is the non-detection of WR 40 in X-rays. This is an important result because it has a slow terminal wind speed v_∞ = 650 - 840 km s^{-1} (Hamann et al. 2006; Gosset et al. 2005) and thus a high average wind density. This may be a clue that X-ray emission ceases to be efficient (or becomes totally absorbed by the wind) in WN stars with slow dense winds.

X-ray observations of a larger sample of single WN stars spanning a broader range of mass-loss parameters are needed to firmly establish any dependencies between L_X and wind parameters. Observations of more WNL stars with slow winds ($v_\infty < 1000$ km s^{-1}) would be particularly useful.

4.6. Comments and Questions on Binarity

Previous X-ray studies have shown that several WR + OB or WR + WR binaries have very high X-ray luminosities with typical values log $L_X \gtrsim 33.0$ ergs s^{-1}. Early evidence for this was found from *Einstein* observations of WR stars. The median X-ray luminosity of seven WN binaries detected by *Einstein* was log L_X(0.2 - 4 keV) = 32.92 ergs s^{-1}, with a range of 32.76 - 33.53 ergs s^{-1} (Pollock 1987). More recent work has confirmed high X-ray luminosities in other WN binary systems. For example, *XMM-Newton* observations of the WN8 + OB system WR 147 gave log L_X(0.5 - 10 keV) = 32.83 ergs s^{-1} (Skinner et al. 2007). A *Chandra* observation of the massive WN binary system WR 20a in Westerlund 2 yielded log L_X = 33.69 ergs s^{-1} based on 1T spectral fits (Nazé et al. 2008). Our analysis of the WR 20a *Chandra* data with 2T *vapec* models gives even higher values log L_X(0.3 - 8 keV) > 34.0 ergs s^{-1} for d > 2.37 kpc. The closely-spaced WN5 + O6 binary V444 Cyg (= WR 139) is also worthy of mention because of its short ≈4.2 d orbital period. *ASCA* observations show that its X-ray luminosity varies with orbital phase, reaching maximum values log L_X(0.7 - 10 keV) > 33.1 ergs s^{-1} for an assumed distance of 1.7 kpc (Maeda et al. 1999).

Thus, there is no doubt that *some* WR binaries are X-ray luminous. But, are *all* WR binaries X-ray luminous? We do not yet know the answer to that question because it can be very difficult to distinguish a closely-spaced binary from a single WR star. It is very likely that some WR stars currently classified as single objects are in fact close unresolved binaries.

Also, a high X-ray luminosity is not strictly required in a colliding wind WR binary system. For an adiabatic colliding wind system the luminosity scales roughly as $L_X \propto \dot{M}^2 v^{-3.2} D^{-1}$ where $\dot{M}$ and v are the mass-loss rate and wind-speed of the dominant component and D is the binary separation (Luo et al. 1990; Stevens et al. 1992). Binaries with lower mass-loss rates or wide separations are expected to have lower L_X, all other factors being equal.

Based on the above, which WN stars in our sample are good binary candidates? WR 24 would appear to be a very good candidate because of absorption lines in its optical spectrum (vdh01) and its high L_X and L_{bol}. In fact, its position in the (L_{bol},L_X) diagram is almost identical to that of the known binary WR 147 (Fig. 9). WR 20b is also a good candidate because of its exceptionally high X-ray luminosity, even when computed using the lowest current distance estimate of d = 2.37 kpc. Searches for close companions in these two stars are certainly justified.

Apart from WR 20b and WR 24, there are no other stars in our sample having high log $L_X \gtrsim 33.0$ ergs s^{-1} that could signal binarity. A particularly interesting case is WR 79a (WN9ha). This star would seem to be a good candidate for binarity based on absorption lines in its spectrum and the possible presence of nonthermal radio emission (Cappa et al. 2004). But its X-ray luminosity log $L_X = 32.14$ ergs s^{-1} is at the low end of the detected WN stars. If WR 79a is indeed a binary then its L_X is much less than other known WN binaries, or its distance has been underestimated.

WR 134 is another intriguing example. Based on its known 2.25 day spectroscopic variability it would seem to rank as a strong binary candidate. As noted in Section 4.4, the high temperature of its hot X-ray component is indeed consistent with that expected if the wind of WR 134 were shocking onto a companion at terminal speed. But there are questions as to whether the X-rays could escape if produced in a closely-spaced colliding wind binary system, and the X-ray luminosity of WR 134 (log $L_X = 32.66$ ergs s^{-1}) is not as high as other known WN binaries. Thus, the existing X-ray data for WR 134 do not provide an indisputable case for binarity. Further observations of WR 134 aimed at determining whether its X-ray emission is modulated at the 2.25 day optical period would be useful since colliding wind binaries such as γ^2 Velorum and WR 140 do show orbital X-ray modulation (Willis, Schild, & Stevens 1995; Zhekov & Skinner 2000; Pollock et al. 2005).

4.7. WN Stars versus WC Stars: A Sharp Contrast in X-rays

Our pilot survey has so far detected all four WN stars observed. In contrast, X-ray observations at similar sensitivity levels did not detect any of the four WC stars in our

sample, and a fifth went undetected in another *XMM-Newton* program (Sec. 1). Why is it that most WN stars are detected as X-ray sources, but WC stars are not?

An important clue to solving this puzzle may lie in the excess X-ray absorption seen in the spectra of most of the WN stars (Sec. 4.1). Such excess absorption has been seen in other WN stars such as WR 6 (WN4; Skinner et al. 2002b). The wind is likely responsible for most of this excess. X-rays produced within the wind must overcome the wind opacity to escape, and the opacity increases toward lower photon energies, all other factors being equal. Thus, softer X-ray photons will be more heavily absorbed and the softest photons detected will have emerged from the wind at large distances from the star.

The wind opacity in WC stars is much higher than in WN stars due to metal-enrichment. For a given set of mass-loss parameters, X-rays of a given energy will have more difficulty escaping a WC wind than a WN wind. As a specific example, we consider a generic WR star with a typical mass-loss rate of $\dot{M} = 2 \times 10^{-5}$ $M_\odot$ yr^{-1} and $v_\infty = 1800$ km s^{-1}. Adopting canonical WN and WC abundances (VCW86) and BM92 cross-sections, the radius of optical depth unity for an X-ray photon of energy E = 1 keV is $\sim$13 times greater for a WC star than for a WN star. Even at higher energies E = 3 keV the $R_{\tau=1}$ ratio is still a factor of $\sim$11. Thus, unless X-rays of moderate energy E $\approx$ 1 - 3 keV are formed very far out in the wind of a WC star (at thousands of solar radii) they will be absorbed. This is perhaps the most plausible explanation for the absence of WC star X-ray detections at present. But a larger sample of WC stars needs to be observed in order to determine if hard X-rays might escape through the wind in some cases. The best candidates for such observations would be WC stars with higher T_{eff} and lower wind densities (lower $\dot{M}$ and higher v_∞), which would conspire to reduce wind opacity.

5. Summary

The most important results of this study are the following:

1. X-ray emission has been detected from four recently-observed WN stars ranging in spectral type from WN2 - WN9, none of which is so far known to be a binary system. Archive data provide detections for an additional three WN6h stars. It is thus now established that both WNE and WNL stars are X-ray sources.

2. The spectra of all stars are similar. All show an admixture of cool ($kT_1 < 1$ keV) and hot ($kT > 2$ keV) X-ray plasma and prominent emission lines from ions such as Si XIII and S XV. X-ray luminosities are typically $\log L_X \sim 32.5$ ergs s^{-1}, but there is a rather large scatter of ± 1 dex around this value. Some of this scatter is likely due to uncertain distances for many WR stars.

3. Most of the detected WN stars show X-ray absorption in excess of that expected from published A_V estimates (WR 2 being an exception). A plausible explanation for the excess absorption is that the X-rays are formed within the wind and are strongly absorbed by the wind at lower energies.

4. The presence of high-temperature plasma in supposedly single WN stars is not predicted by radiative wind shock models. Other mechanisms are thus required to explain the hotter plasma. Close companion models are not clearly justified given the lack of evidence for binarity. Magnetic wind confinement models provide some promise, but the presence of magnetic fields in WR stars has so far not been demonstrated. Further theoretical work is needed to develop models that can account for such hot plasma.

5. Although the sample of WN stars observed in X-rays is small, there is a noticeable trend toward lower L_X in the later WN7-9 subtypes. This is in the opposite sense of L_{bol}, which increases toward later WN7-9 subtypes. Thus, other factors besides L_{bol} determine X-ray luminosity in single WN stars. Wind properties appear to be important, and sensitive X-ray observations of a broader sample of WN stars, particularly at low terminal wind speeds, are needed to determine if L_X depends on wind parameters.

This work was supported by *Chandra* award GO8-9008X issued by the Chandra X-ray Observatory Center (CXC) and by NASA/GSFC award NNX09AR25G. The CXC is operated by the Smithsonian Astrophysical Observatory (SAO) for, and on behalf of, the National Aeronautics Space Administration under contract NAS8-03060. We acknowledge

use of *Chandra* archive data for WR 24 obtained in a guaranteed time observation (GTO ObdId 9482, PI G. Garmire). This observation was part of a larger *Chandra* ACIS survey of the Carina Nebula (Chandra Carina Complex Project; PI: L. Townsley). This work was partially based on observations obtained with XMM-Newton, an ESA science mission with instruments and contributions directly funded by ESA member states and the USA (NASA). SZ acknowledges financial support from Bulgarian National Science Fund grant DO-02-85.

Table 1. WN Star Properties

Name	Sp. Type	d (kpc)	A_V (mag)	v_∞ (km/s)	$\dot{M}$ (10^{-5} $M_\odot$/yr)	R_* ($R_\odot$)	log L_{bol} ($L_\odot$)
			New Detections[a]				
WR 2	WN2	2.51	1.58	3200[b]	$\leq$2.0[c]	0.89	5.45
WR 18	WN4	2.20	2.63	1800	2.5	1.49	5.50
WR 79a	WN9ha	1.99	1.28	955	2.4[d]	33.1	5.78
WR 134	WN6	1.74	1.52	1820[e]	4.0	5.29	5.60
			Archive Data[f]				
WR 16	WN8h	2.37	1.80	650	5.0	19.9	6.15
WR 20b	WN6h	$\geq$2.37	6.08	...	...	...	5.86[g]
WR 24	WN6ha	3.24	0.56	2160	4.0	19.9	6.35
WR 78	WN7h	1.99	1.50	1385	5.0	16.7	6.20
WR 136	WN6h	1.64[h]	1.73	1600	3.2	3.3	5.40

[a]Spectral type, distance and A_V from vdH01 (A_v=1.11 A_V). For WR 2, WR 18, WR 134: v_∞, $\dot{M}$, R_*, L_{bol} from Hamann et al. (2006), unless otherwise noted. For WR 79a: v_∞, $\dot{M}$, R_*, L_{bol} from Crowther & Bohannan (1997).

[b]Howarth & Schmutz (1992) obtained v_∞ = 3200 km s^{-1}. Hamann et al. (2006) give v_∞ = 1800 km s^{-1}.

[c]Upper limit is based on a *VLA* non-detection with a 6 cm flux density S_{6cm} <0.2 mJy (Abbott et al. 1986) and v_∞ = 3200 km s^{-1}.

[d]Spectroscopic mass-loss rate (Crowther & Bohannan 1997).

[e]Ignace et al. (2001).

[f]For archive objects, the spectral type, distance, and A_V are from vdH01 and other properties from Hamann et al. (2006), unless otherwise noted. No mass-loss data specific for WR 20b were found.

[g] L_{bol} from Nazé et al. (2008).

[h]From *Hipparcos* parallax (0.61 mas).

Table 2. WN Stars: New X-ray Observations

Parameter	WR 2	WR 18	WR 134	WR 79a
Date	2008 June 30	2008 Oct 29	2008 Feb 10	2009 Aug 30
ObsId	8943	8910	8909	0602020101
Start Time (TT)	06:17:17	16:59:38	10:23:29	01:44:03
Stop Time (TT)	11:17:51	23:06:05	16:31:11	11:59:17
Exposure (s)	15,444	19,684	19,301	35,033 (pn), 36,617 (per MOS)
Instrument	ACIS-S	ACIS-S	ACIS-S[a]	EPIC
Frametime (s)	3.1	3.1	0.9	0.073 (pn), 2.6 (MOS)

[a]WR 134 observed using 1/4 subarray to mitigate pileup.

Table 3. WN Star X-ray Source Properties[a]

Name	R.A. (J2000)	Decl. (J2000)	Net Counts (cts)	Rate (cts/ksec)	E_{50} (keV)	P_{const}	Identification(offset) (arcsec)
			New Detections				
WR 2	01 05 23.05	+60 25 18.9	247±16	16.0±1.04	1.04	0.68 (0.92)	HST J010523.02+602518.9 (0.22)
WR 18	10 17 02.26	-57 54 46.8	167±13	8.48±0.66	1.67	0.99 (0.91)	HST J101702.28−575446.9 (0.19)
WR 79a	16 54 58.52	-41 09 02.9	805±29[b]	23.0±0.83[b]	1.35	0.63 (...)	HST J165458.50−410903.1 (0.30)
WR 134	20 10 14.19	+36 10 35.1	785±28	40.7±1.45	1.90	0.95 (0.95)	HST J201014.19+361035.1 (0.00)
			Chandra Archive Detections				
WR 20b[c]	10 24 18.39	-57 48 29.9	643±26	13.0±0.53	3.04	0.24 (0.93)	HST J102418.41−574829.7 (0.26)
WR 24[d]	10 43 52.24	-60 07 04.2	1419±39	25.1±0.69	1.66	0.67 (0.97)	HST J104352.26−600704.0 (0.18)
WR 136[e]	20 12 06.56	+38 21 18.2	238±17	2.56±0.18	1.96	0.99 (0.93)	HST J201206.54+382117.8 (0.46)

[a]Notes: *Chandra* X-ray data for WR 2, WR 18, WR 134, and WR 136 are from ACIS-S and WR 20b, WR 24 are from ACIS-I. *XMM-Newton* data for WR 79a are from EPIC pn. Parameters were determined using events in the 0.3 - 8 keV range. Tabulated quantities are: source name, J2000.0 X-ray position (R.A., Decl.), net counts and net counts error (from 3σ *wavdetect* ellipses for *Chandra* sources and from a 90% encircled energy circular source region of radius r = 45″ for the *XMM* source WR79a, accumulated in the exposure given in Table 2, rounded to the nearest integer, background subtracted and PSF-corrected), count rate (Rate) obtained by dividing net counts by the exposure time in Table 2, median photon energy E_{50}, probability of constant count-rate (P_{const}) from the KS test followed in parentheses by the corresponding probability from the Gegory-Loredo method for *Chandra* sources as determined from the CIAO tool *glvary*, and HST GSC v2.3.2 optical counterpart identification within a 2″ search radius. The offset (in arcsecs) between the X-ray and optical counterpart position is given in parentheses.

[b]The corresponding EPIC MOS values in the 0.3 - 8 keV range using a r = 45″ source extraction region are: MOS1 286 ± 17 net counts, 7.81 ± 0.46 c/ksec; MOS2 281 ± 17 net counts, 7.67 ± 0.46 c/ksec.

[c]*Chandra* ObsID 6411, 49,377 s exposure on 28 Sept. 2006 ;WR 20b positioned ≈4.1′ off-axis.

[d]*Chandra* ObsID 9482, 56,519 s exposure on 18 Aug. 2008; WR 24 positioned ≈7.4′ off-axis.

[e]*Chandra* ObsID 3763, 92,771 s exposure on 19 Feb. 2003; WR 136 positioned ≈8.2′ off-axis.

Table 4. X-ray Spectral Fits of WN Stars (New Detections)

Parameter	Object			
Star	WR 2	WR 18	WR 134	WR79a
Model	2T vapec	2T vapec	2T vapec	2T vapec
Abundances[a]	WN[b]	WN[c]	WN[d]	WN[e]
N_H (10^{22} cm^{-2})	0.44 [0.08 - 0.99]	1.37 [0.72 - 1.86]	1.19 [0.83 - 1.45]	0.75 [0.64 - 0.83]
kT_1 (keV)	0.32 [0.24 - 0.45]	0.65 [0.43 - 0.82]	0.62 [0.53 - 0.71]	0.55 [0.46 - 0.61]
$norm_1$ (10^{-6})	1.73 [0.99 - 70.0]	2.24 [0.45 - 7.85]	1.47 [0.34 - 3.70]	2.04 [1.39 - 3.16]
kT_2 (keV)	$\geq$2.6[f]	3.51 [1.86 - ...]	8.57 [5.74 - 17.2]	2.66 [1.66 - 5.60]
$norm_2$ (10^{-6})	0.56 [0.14 - 0.89]	0.85 [0.33 - 1.48]	3.75 [1.66 - 5.04]	0.47 [0.27 - 0.73]
χ^2/dof	17.2/14	4.0/7	57.6/56	46.4/48
χ^2_{red}	1.23[g]	0.57	1.03	0.97
F_X (10^{-13} ergs cm^{-2} s^{-1})	0.86 (4.56)	0.58 (4.87)	4.36 (12.5)	0.64 (2.94)
$F_{X,1}$ (10^{-13} ergs cm^{-2} s^{-1})	0.37 (3.96)	0.22 (4.16)	0.68 (7.20)	0.41 (2.53)
log L_X (ergs s^{-1})	32.54	32.45	32.66	32.14
log [L_X/L_{bol}]	−6.49	−6.63	−6.52	−7.22
log [L_X/L_{wind}]	$\geq$−5.27	−4.96	−4.96	−4.70
$N_H/N_{H,vis}$	1.3 [0.2 - 2.8]	2.3 [1.2 - 3.2]	3.5 [2.5 - 4.3]	2.6 [2.2 - 2.9]

Note. — Based on XSPEC (vers. 12.4.0) fits of the background-subtracted spectra binned to a minimum of 10 counts per bin using the optically thin thermal plasma *vapec* model. All models included the XSPEC *wabs* photoelectric absorption component, based on Morrison & McCammon (1983) cross-sections and Anders & Ebihara (1982) relative abundances. The tabulated parameters are equivalent neutral H absorption column density (N_H), the product of Boltzmann's constant time plasma temperature (kT), and XSPEC component normalization (norm). Square brackets enclose 90% confidence intervals and an ellipsis means that the algorithm used to compute confidence intervals did not converge. The total X-ray flux (F_X) and flux of the cool component ($F_{X,1}$) are the absorbed values in the 0.3 - 8 keV range, followed in parentheses by unabsorbed values. The unabsorbed luminosity L_X (0.3 - 8 keV) assumes the distances given in Table 1. L_{bol} is from Table 1. $L_{wind} = (1/2)\dot{M}v_\infty^2$ (Table 1). The ratio $N_H/N_{H,vis}$ of X-ray to optically-derived absorption is computed using $N_{H,vis} = 2.22 \times 10^{21} A_V$ cm^{-2} (Gorenstein 1975), where A_V is from Table 1.

[a]Abundances were held fixed at the generic WN values given in Table 1 of VCW86, except for specific elements whose abundances were allowed to vary as noted below. The generic WN abundances reflect H depletion and N enrichment and are by number: He/H = 14.9, C/H = 1.90E-03, N/H = 9.36E-02, O/H = 4.35E-03, Ne/H = 9.78E-03, Mg/H = 3.26E-03, Si/H = 3.22E-03, P/H = 1.57E-05, S/H = 7.60E-04, Fe/H = 1.90E-03. All other elements were held fixed at solar abundances (Anders & Grevesse 1989).

[b]The abundances of N, Mg, and Fe were varied to improve the fit and converged to values N = 5.3, Mg = 2.1, and Fe = 1.3 times the number ratios given in VCW86. The S abundance is poorly constrained and was held fixed at S = 3.0 times the number ratio given in VCW86.

[c]The abundances of Mg and Fe were varied to improve the fit and converged to values Mg = 0.3, and Fe = 2.1 times the number ratios given in VCW86.

[d]The abundances of Mg, Si, S, and Fe were varied to improve the fit and converged to values Mg = 3.3, Si = 6.0, S = 18.6, and Fe = 5.6 times the number ratios given in VCW86.

[e]The abundances of Si, S, and Ne were varied to improve the fit and converged to values Si = 2.7, S = 8.4, Ne = 0.46 times the number ratios given in VCW86. A solar abundance 2T *vapec* fit underestimates the Si XIII line flux, but allowing the Si abundance to vary gives an acceptable fit with Si = 3.4 × solar. The temperatures inferred from the solar abundance fit are nearly identical to those with WN abundances, but solar abundances

converge to an N_H value that is 20% larger and give a slightly larger log L_X = 32.3 ergs s^{-1}.

[f] Lower bound is 90% confidence. The value of kT_2 is sensitive to the S abundance and not tightly-constrained.

[g]Some further reduction in χ^2_{red} can be obtained by allowing the S abundance to increase to very large values.

Table 5. X-ray Spectral Fits of WN6 Stars (*Chandra* Archive Data)

Parameter	Object		
Star	WR 20b	WR 24	WR 136
Model	2T vapec	2T vapec	2T vapec
Abundances[a]	WN[b]	WN[c]	WN[d]
$N_{H,1}$ (10^{22} cm^{-2})	3.92 [2.96 - 7.45]	0.82 [0.43 - 1.06]	0.49 [0.36 - 0.72]
kT_1 (keV)	0.44 [0.28 - 0.75]	0.70 [0.64 - 0.83]	0.56 [0.33 - 0.73]
$norm_1$ (10^{-6})	54.6 [24.9 - 76.0]	5.61 [1.63 - 8.88]	20.3 [10.2 - 103.]
$N_{H,2}$ (10^{22} cm^{-2})	...	...	3.98 [1.63 - 7.41]
kT_2 (keV)	5.43 [3.16 - 9.09]	3.33 [2.48 - 4.83]	2.64 [1.53 - 18.0]
$norm_2$ (10^{-6})	5.56 [4.46 - 8.23]	3.22 [2.32 - 4.36]	87.0 [59.8 - 205.]
χ^2/dof	55.6/50	110.2/99	49.6/46
χ^2_{red}	1.11[e]	1.11	1.08
F_X (10^{-13} ergs cm^{-2} s^{-1})	2.27 (60.6)	2.51 (7.95)	0.29 (1.02)
$F_{X,1}$ (10^{-13} ergs cm^{-2} s^{-1})	0.32 (56.0)	1.10 (5.45)	0.07 (0.27)
log L_X (ergs s^{-1})	$\geq$33.57	33.0	31.51
$N_{H,1}/N_{H,vis}$	2.9 [2.2 - 5.5]	6.6 [3.5 - 8.5]	1.3 [0.9 - 1.9]
$N_{H,2}/N_{H,vis}$	...	...	10.4 [4.2 - 19.3]

Note. — Based on XSPEC (vers. 12.4.0) fits of the background-subtracted spectra binned to a minimum of 10 counts per bin using the optically thin thermal plasma *vapec* model. The tabulated parameters are the same as in Table 4. Square brackets enclose 90% confidence intervals. The total X-ray flux (F_X) and flux of the cool component ($F_{X,1}$) are the absorbed values in the 0.3 - 8 keV range, followed in parentheses by unabsorbed values. The unabsorbed luminosity L_X (0.3 - 8 keV) assumes the distances given in Table 1.

[a]Abundances were held fixed at the generic WN values given in Table 1 of VCW86, except for specific elements whose abundances were allowed to vary as noted below. The generic WN abundances are given in Table 4.

[b]The abundances of Mg, Si, and S were varied to improve the fit and converged to values Mg = 0.6, Si = 0.2, and S = 3.0 times the number ratios given in VCW86.

[c]The abundances of Mg, Si, S, and Fe were varied to improve the fit and converged to values Mg = 0.9, Si = 1.1, S = 5.2, and Fe = 0.6 times the number ratios given in VCW86.

[d]The abundances of Si and S were varied to improve the fit and converged to values Si = 2.6 and S = 5.4 times the number ratios given in VCW86.

[e]A slightly better fit can be obtained using the plane-parallel shock model *vpshock*. This fit converges to N_H = 4.67 [3.67 - 6.11] × 10^{22} cm^{-2}, kT_{shock} = 3.86 [2.97 - 6.53] keV, Mg = 1.7, Si = 0.3, S = 1.6 times the number ratios given in VCW86, χ^2/dof = 45.5/51, χ^2_{red} = 0.89, F_X(0.3 - 8 keV) = 2.09 (97.1) × 10^{-13} ergs cm^{-2} s^{-1}, log L_X = 33.78 ergs s^{-1} (d = 2.27 kpc).

REFERENCES

Abbott, D.C., Bieging, J.H., Churchwell, E., & Torres, A.V. 1986, ApJ, 303, 239

Anders, E., & Ebihara, M. 1982, Geochim. Cosmochim. Acta, 46, 2363

Anders, E., & Grevesse, N. 1989, Geochim. Cosmochim. Acta, 53, 197

Arnal, E.M., Cappa, C.E., Rizzo, J.R., & Cichowolski, S. 1999, AJ, 118, 1798

Babel, J. & Montmerle, T., 1997, A&A, 323, 121

Balucińska-Church, M. & McCammon, D. 1992, ApJ, 400, 699 (BM92)

Baum, E., Hamann, W.-R., Koesterke, L. & Wessolowski, U. 1992, A&A, 266, 402

Berghöfer, T.W., Schmitt, J.H.M.M., Danner, R., & Cassinelli, J.P., 1997, A&A, 322, 167

Bieging, J.H., Abbott, D.C., & Churchwell, E.B., 1989, ApJ, 340, 518

Bochkarev, N.G. 1988, Nature, 332, 518

Borkowski, K.J., Lyerly, W.J., & Reynolds, S.P. 2001, ApJ, 548, 820

Cappa, C., Goss, W.M., & van der Hucht, K.A. 2004, AJ, 127, 2885

Cassinelli, J.P., Miller, N.A., Waldron, W.A., MacFarlane, J.J., & Cohen, D.H., 2001, ApJ, 554, L55

Chu, Y.-H., Gruendl, R.A., & Guerrero, M.A. 2006, in The X-ray Universe 2005 (ESA SP-604), ed. A. Wilson, 363

Chu, Y.-H., Treffers, R.R., & Kwitter, K.B. 1983, ApJS, 53, 937

Cohen, D.H., Kuhn, M.A., Gagné, M., Jensen, E.L.N., & Miller, N.A. 2008, 386, 1855

Crowther, P.A. 2007, ARA&A, 45, 177

Crowther, P.A. & Bohannan, B. 1997, A&A, 317, 532

Davidson, K. & Ostriker, J.P. 1973, ApJ, 179, 585

Dyson, J.E. & Ghanbari, J. 1989, A&A, 226, 270

Feldmeier, A., Kudritzki. R.-P., Palsa, R. Pauldrach, A.W.A., & Puls, J., 1997, A&A, 320, 899

Firmani, C., Koenigsberger, G., Bisiacchi, G.F., Moffat, A.F.J., & Isserstedt, J. 1980, ApJ, 239, 607

Gayley, K.G. & Owocki, S.P., 1995, ApJ, 446, 801

Gorenstein, P. 1975, ApJ, 198, 95

Gosset, E., Nazé, Y., Claeskens, J.-F., Rauw, G., Vreux, J.-M., & Sana, H. 2005, A&A, 429, 685

Gregory, P.C. & Loredo, T.J. 1992, ApJ, 398, 146

Gregory, P.C. & Loredo, T.J. 1996, ApJ, 473, 1059

Gruendl, R.A., Chu, Y.-H., Dunne, B.C., & Points, S.D. 2000, ApJ, 120, 2670

Gruendl, R.A., Guerrero, M.A., & Chu, Y.-H. 2003, BAAS, 35, 746

Hamann, W.-R., Gräfener, G. & Liermann, A. 2006, A&A, 457, 1015

Howarth, I.D. & Schmutz, W. 1992, A&A, 261, 503

Ignace, R., Cassinelli, J.P., Quigley, M., & Babler, B. 2001, ApJ, 558, 771

Ignace, R., Oskinova, L.M., & Brown, J.C. 2003a, A&A, 408, 353

Ignace, R., Quigley, M.F., & Cassinelli, J.P. 2003b, ApJ, 596, 538

Kahn, S.M. et al., 2001, A&A, 365, L312

Lépine, S. et al. 2000, AJ, 120, 3201

Lipunov, V.M. 1982, Sov. Astron. Lett., 8, 194

Lommen, D., Yungelson, L., van den Heuvel, E., Nelemans, G., & Zwart, S.P. 2005, A&A, 443, 231

Lucy, L.B., 1982, ApJ, 255, 286

Lucy, L.B. & White, R.L., 1980, ApJ, 241, 300

Luo, D., McCray, R., & MacLow, M-M., 1990, ApJ, 362, 267

Maeda, Y., Koyama, K., Yokogawa, J., & Skinner, S. 1999, ApJ, 510, 967

Marston, A.P. 2001, ApJ, 563, 875

Marston, A.P. 2003, in *A Massive Star Odyssey, from Main Sequence to Supernova* (IAU Symp. No. 212), eds. K.A. van der Hucht, A. Herrero, & C. Estaban (San Francisco: ASP), 732

Mason, B.D. Gies, D.R., Hartkopf, W.I., Bagnuolo, W.G., Brummelaar, T.t., & McAlister, H.A. 1998, AJ, 115, 821

Miller, G.J. & Chu, Y.-H. 1993, ApJS, 85, 137

Miller, N.A., Cassinelli, J.P., Waldron, W.L., MacFarlane, J.J., & Cohen, D.H. 2002, ApJ, 577, 951

Moffat, A.F.J., Drissen, L., Lamontagne, R., & Robert, C. 1988, ApJ, 334, 1038

Morel, T. et al. 1999, ApJ, 518, 428

Morrison, R. & McCammon, D. 1983, ApJ, 270, 119

Nazé, Y., Rauw, G., & Manfroid, J. 2008, A&A, 483, 171

Oskinova, L.M. 2005, MNRAS, 361, 679

Oskinova, L.M., Ignace, R., Hamann, W.-R., Pollock, A.M.T., & Brown, J.C. 2003, A&A, 402, 755

Owocki, S.P., Castor, J.I., & Rybicki, G.B., 1988, ApJ, 335, 914

Owocki, S.P. & Cohen, D.H. 2001, ApJ, 559, 1108

Owocki, S.P. & Cohen, D.H. 1999, ApJ, 520, 833

Pollock, A.M.T. 1987, ApJ, 320, 283

Pollock, A.M.T., Corcoran, M.F., Stevens, I.R., & Williams, P.M. 2005, ApJ, 629, 482

Press, W.H., Teukolsky, S.A., Vetterling, W.T., & Flannery, B.P. 1992, Numerical Recipes in Fortran: The Art of Scientific Computing (2nd ed.; New York: Cambridge Univ. Press), 617

Prilutskii, O.F. & Usov, V.V. 1976, Soviet Ast., 20, 2

Robert, C. 1994, Ap&SS, 221, 137

Schild, H. et al. 2004, A&A, 422, 177

Schmutz, W. 1997, A&A, 321, 268

Schmutz, W., Geballe, T.R., & Schild, H. 1996, A&A, 311, L25

Schulte-Ladbeck, R.E., Nordsieck, K.H., Taylor, M., Bjorkman, K.S., Magalhaes, A.M., & Wolff, M.J. 1992, ApJ, 387, 347

Schulz, N.S., Canizares, C.R., Huenemoerder, D., & Lee, J.C., 2000, ApJ, 545, L135

Seward, F.D., Forman, W.R., Giacconi, R., Griffiths, R.E., Harnden, F.R., Jones, C., & Pye, J.P. 1979, ApJ, 234, 55

Skinner, S.L., Güdel, M., Schmutz, W., & Stevens, I.R., 2001, ApJ, 558, L113

Skinner, S.L., Güdel, M., Schmutz, W., & Zhekov, S. 2006, Astrophys. Space Sci., 304, 97

Skinner, S.L., Sokal, K.R., Cohen, D.H., Gagné, M., Owocki, S.P., & Townsend, R.H. 2008, ApJ, 683, 796

Skinner, S.L., Zhekov, S., Güdel, M., & Schmutz, W. 2002a, ApJ, 572, 477

Skinner, S.L., Zhekov, S., Güdel, M., & Schmutz, W. 2002b, ApJ, 579, 764

Skinner, S.L., Zhekov, S., Güdel, M., & Schmutz, W. 2007, MNRAS, 378, 1491

Skinner, S.L., Zhekov, S., Güdel, M., & Schmutz, W., & Sokal, K. 2009, BAAS, 41, 470

Smith, R.K., Brickhouse, N.S., Liedahl, D.A., & Raymond, J.C. 2001, ApJ, 556, L91

Stevens, I.R., Blondin, J.M., & Pollock, A.M.T., 1992, ApJ, 386, 265

St.-Louis, N., Chené, A.-N., Schnurr, O., & Nicol, M.-H. 2009, ApJ, in press

Strüder, L. et al., 2001, A&A, 365, L18

Turner, M.J.L. et al., 2001, A&A, 365, L27

ud-Doula, A. & Owocki, S.P., 2002, ApJ, 576, 413

Usov, V.V. 1992, ApJ, 389, 635

van den Heuvel, E.P.J. & De Loore, C. 1973, A&A, 25, 387

van der Hucht, K.A., 2001, New Ast. Rev., 45, 135 (vdH01)

van der Hucht, K.A., Cassinelli, J.P., & Williams, P.M., 1986, A&A, 168, 111 (VCW86)

van der Hucht, K.A., Williams, P.M., & Thé, P.S. 1987, QJRAS, 28, 254

Waldron, W. & Cassinelli, J.P., 2009, ApJ, 692, L76

Willis, A.J., Schild, H., & Stevens, I.R. 1995, A&A, 298, 549

Zhekov, S.A. & Skinner, S.L. 2000, ApJ, 538, 808

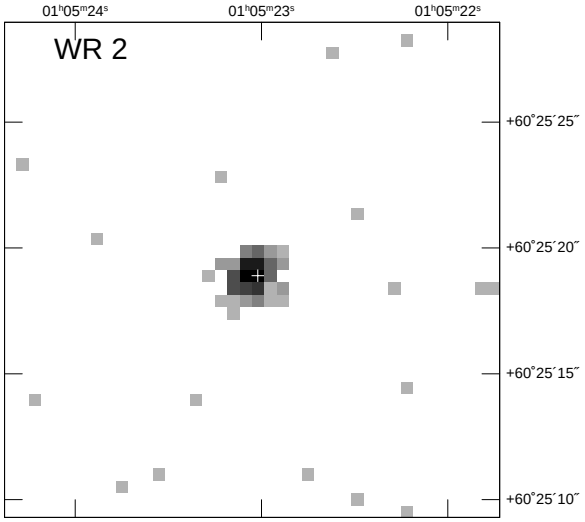

Fig. 1.— *Chandra* ACIS-S image of WR 2 in the 0.3 - 8 keV energy range. The pixel size is 0.″492. The image is displayed on a log intensity scale and the coordinates are J2000.0. The cross marks the *HST* GSC position of WR 2.

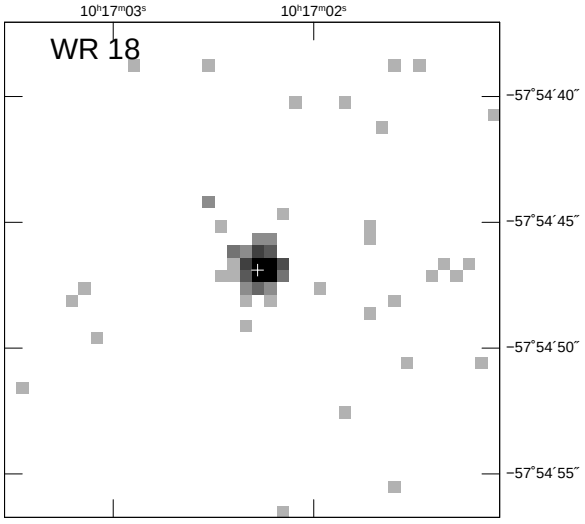

Fig. 2.— *Chandra* ACIS-S image of WR 18 in the 0.3 - 8 keV energy range. Annotation and image properties are the same as in Figure 1.

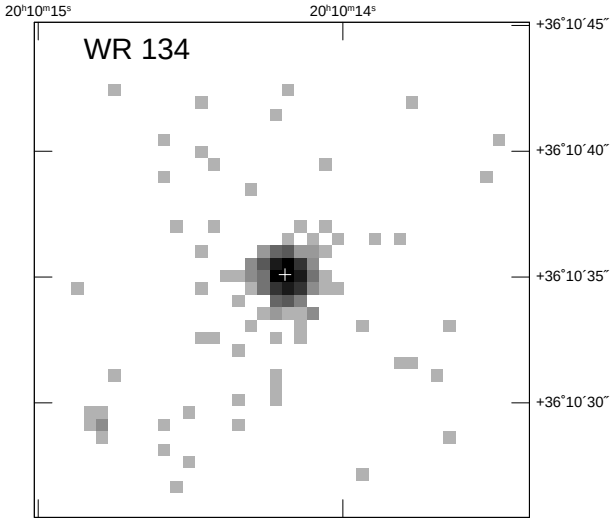

Fig. 3.— *Chandra* ACIS-S image of WR 134 in the 0.3 - 8 keV energy range. Annotation and image properties are the same as in Figure 1.

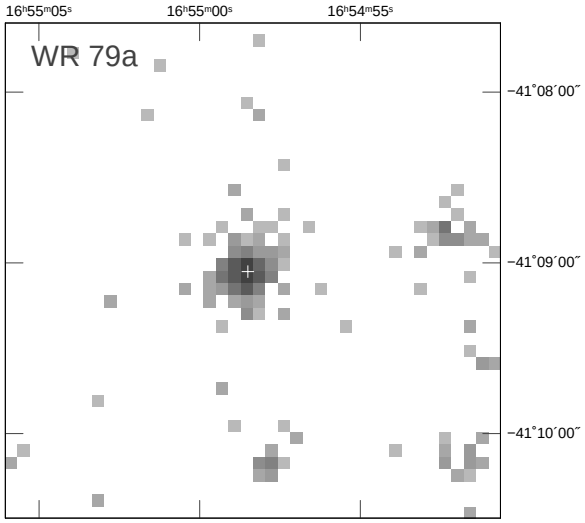

Fig. 4.— *XMM-Newton* EPIC pn image of WR 79a in the 0.3 - 8 keV energy range. The pixel size is 4.″3. The image is displayed on a log intensity scale and the coordinates are J2000.0. The cross marks the *HST* GSC position of WR 79a.

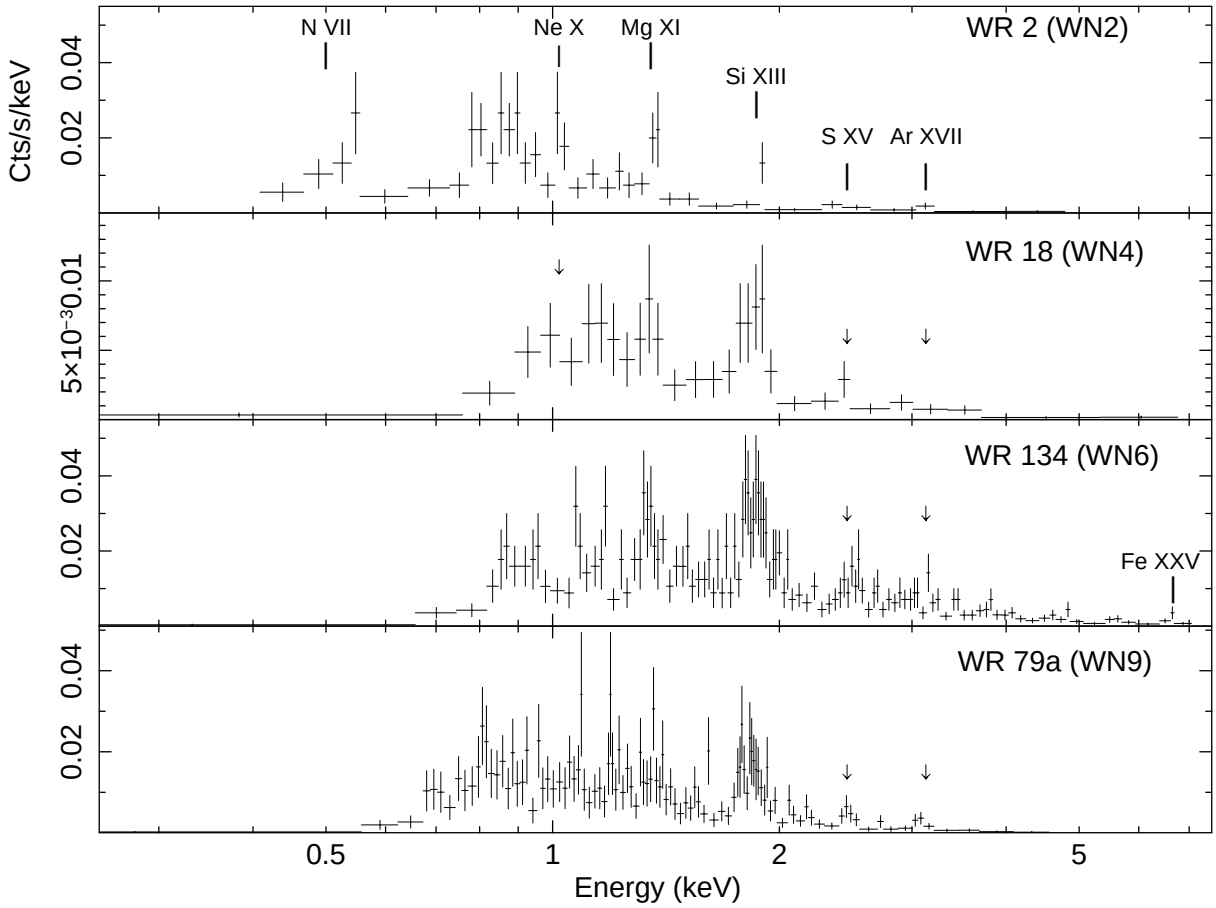

Fig. 5.— *Chandra* ACIS-S spectra of WR 2, WR 18, and WR 134 and *XMM-Newton* EPIC pn spectrum of WR 79a. The spectra are background-subtracted and rebinned to a minimum of 5 counts per bin for display. Prominent emission lines are marked.

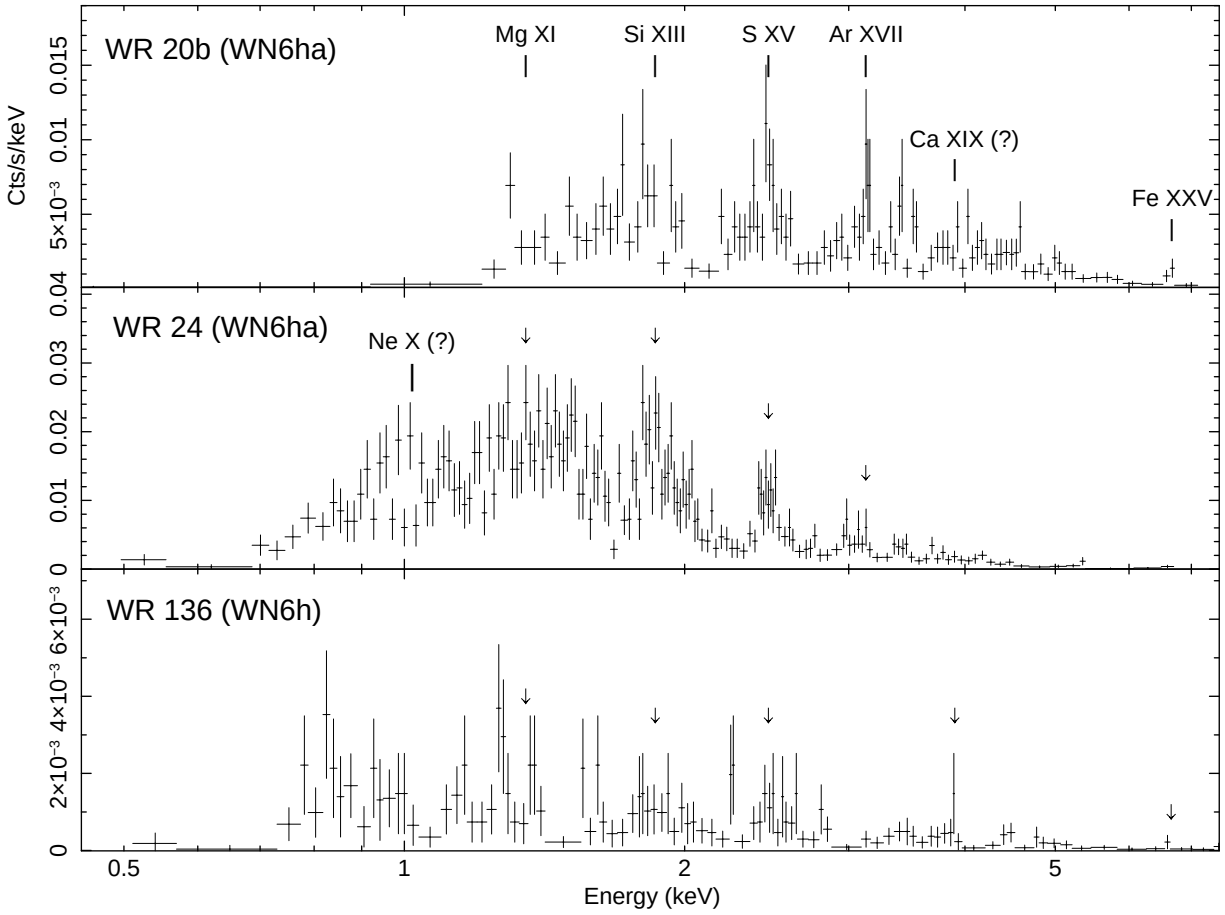

Fig. 6.— Background-subtracted *Chandra* ACIS spectra of WR 20b, WR 24, and WR 136 from archive data. The spectra of WR 20b and WR 24 are rebinned to a minimum of 5 counts per bin, and the fainter source WR 136 is rebinned to a minimum of 2 counts per bin. Prominent emission lines are marked. The Ca XIX line in WR 20b and WR 136 is faint and is classified as a possible detection.

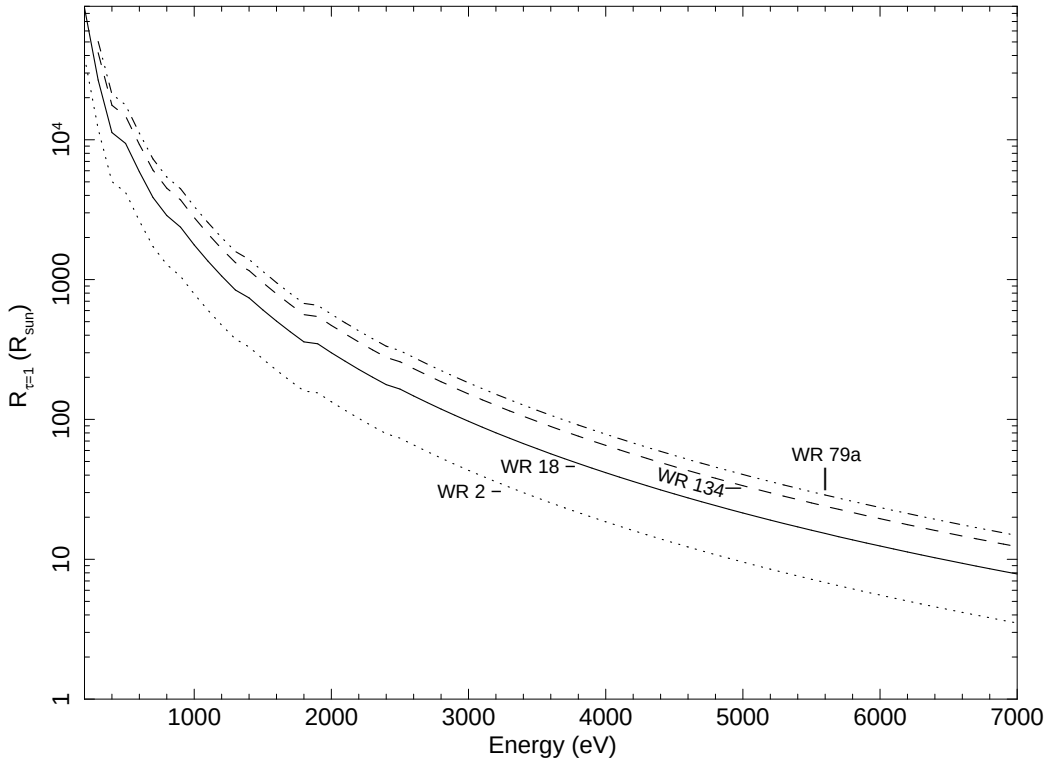

Fig. 7.— Radius of optical depth unity as a function of photon energy for the detected WN stars. The radii are calculated for a spherical constant-velocity wind using the mass-loss parameters in Table 1, generic WN abundances (VCW86), and BM92 cross-sections.

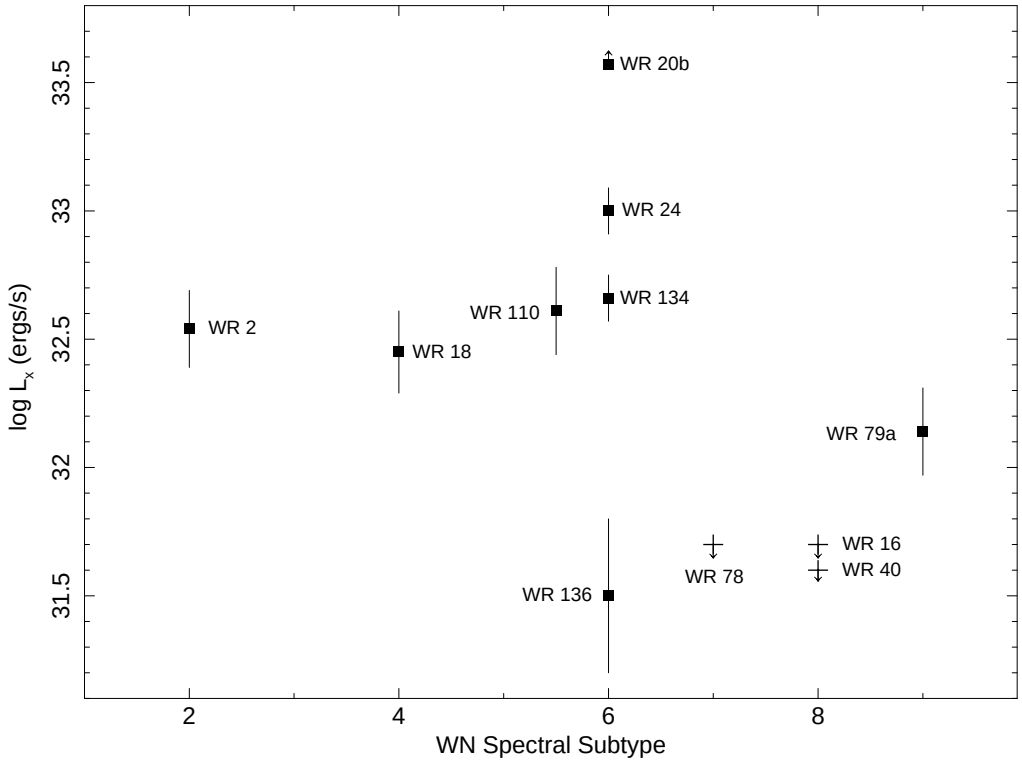

Fig. 8.— X-ray luminosity (Tables 4 and 5) versus spectral subtype for putatively single WN stars. The X-ray data for WR 110 (WN5-6) are from *XMM-Newton* (Skinner et al. 2002a). The X-ray upper limit for WR 40 (WN8) is from *XMM-Newton* (Gosset et al. 2005). The 3σ upper limits for WR 16 (WN8h) and WR 78 (WN7h) are based on analysis of archival *ROSAT* PSPC images (Sec. 3.3). Error bars on L_X are internal only and do not include possible systematic effects such as distance uncertainties.

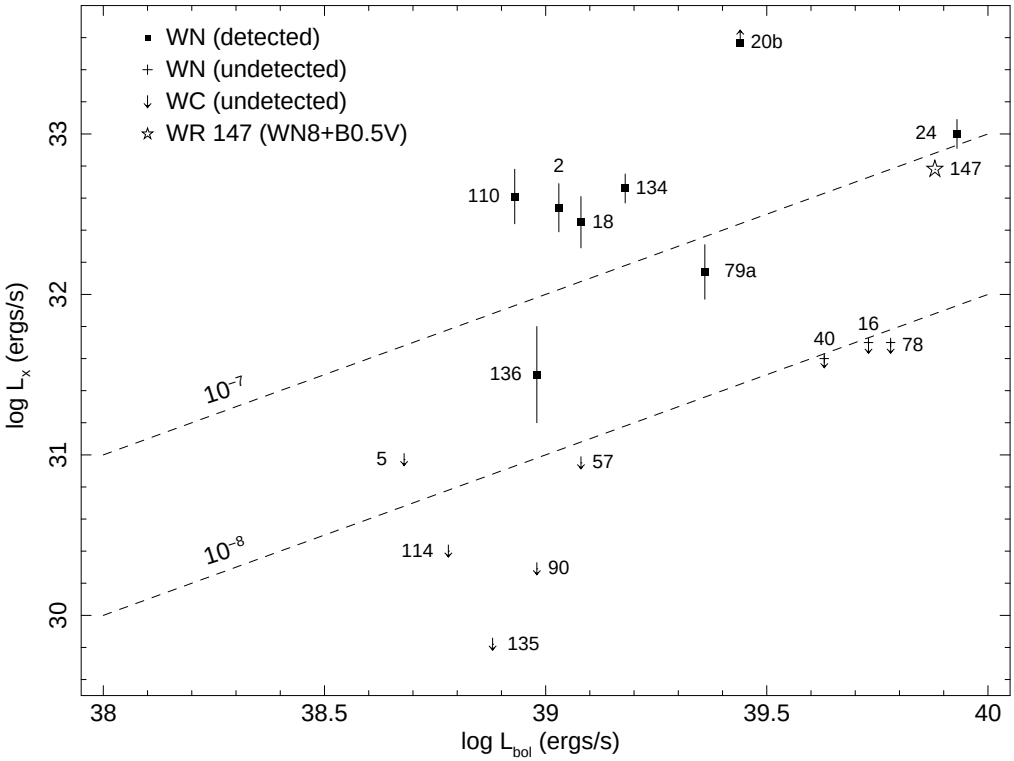

Fig. 9.— X-ray versus bolometric luminosity for suspected single WN and WC stars. The WN + OB binary system WR 147 is also shown for comparison. L_{bol} values are from Hamann et al. (2006) except for WR 79a (Crowther & Bohannan 1997) and WR 20b (Nazé et al. 2008). L_X for detections are from Tables 4 and 5 except for WR 110 (Skinner et al. 2002a) and WR 147 (Skinner et al. 2007). The WN4 star WR 6 (= EZ CMa) is an X-ray source (Skinner et al. 2002b), but is not shown because of an uncertain distance d = 0.58 - 1.8 kpc and suspected binarity. If an intermediate distance d = 1.2 kpc is assumed, it would lie at (L_{bol}, L_X) ≈ (39.18, 32.7), which is nearly coincident with WR 134. Plotted error bars on L_X are internal only and do not account for possible systematic effects such as distance uncertainties. X-ray upper limits for WC stars are from Skinner et al. (2006, 2009), except for WR 114 (Oskinova et al. 2003). The X-ray upper limit for WR 40 is from Gosset et al. (2005). The dashed lines show slopes for reference and are not regression fits.

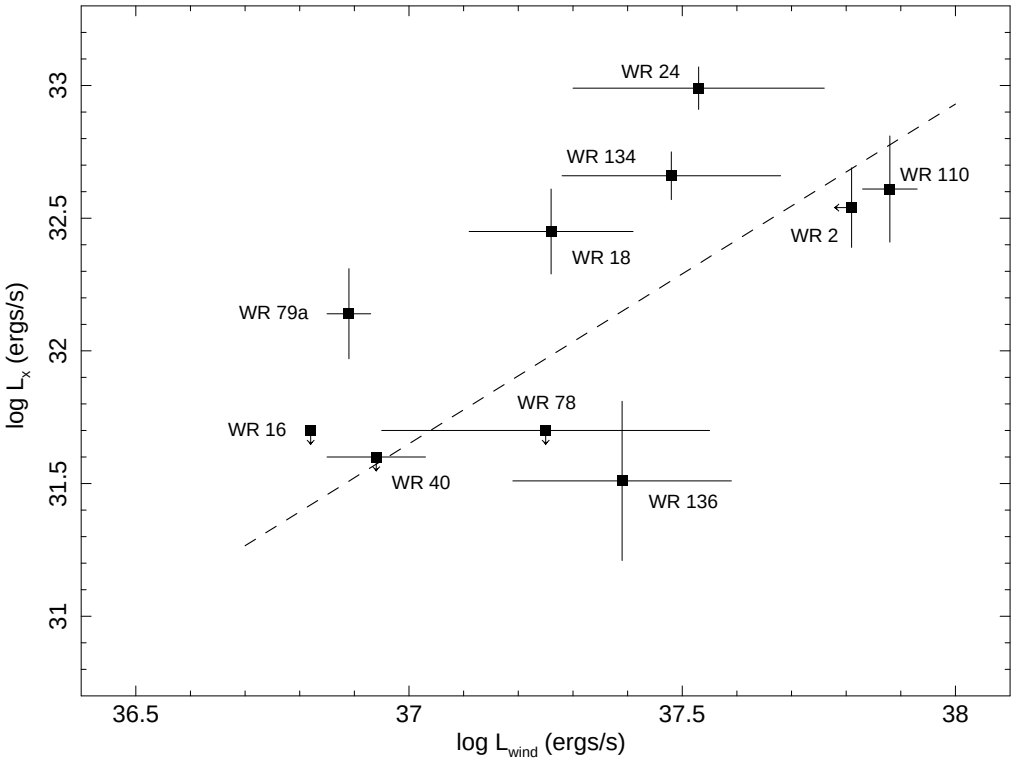

Fig. 10.— X-ray versus wind luminosity ($L_{wind} = \frac{1}{2}\dot{M}v_\infty^2$) for the WN stars in this study. Also included is the WN5-6 star WR 110 using data from Skinner et al. (2002a). WR 20b is excluded for lack of reliable mass-loss data and an uncertain distance. The WN4 star WR 6 (= EZ CMa) is an X-ray source (Skinner et al. 2002b), but is not shown because of an uncertain distance d = 0.58 - 1.8 kpc and suspected binarity. If an intermediate distance d = 1.2 kpc is assumed, along with mass-loss estimates from Schmutz (1997), it would lie at at (L_{wind}, L_X) $\approx$ (37.4, 32.7), which is nearly coincident with WR 134. The X-ray upper limits for WR 16 and WR 78 are from *ROSAT* (Sec. 3.3). The X-ray upper limit for WR 40 is from Gosset et al. (2005). Error bars on L_X are internal only and do not account for possible systematic effects such as distance uncertainties. The plotted values of L_{wind} are log averages based on calculations using published $\dot{M}$ and v_∞ values. The error bars on L_{wind} reflect the spread in published $\dot{M}$ and v_∞ for each star. The dashed line has slope m = +1.28 ± 0.51 and is a regression fit to the data, taking both X-ray detections and upper limits into account. *Notes (and mass-loss references in parentheses):* WR 2: The upper limit on L_{wind} assumes log $\dot{M} \leq -4.7$ (1) computed using $v_\infty = 3200$ km s^{-1} (2); WR 16: (4); WR 18: (3,4); WR 24: (3,4); WR 40: (4,9) WR 78: (3,4); WR 79a: (3,5); WR 134: (1,2,4,6); WR 136: (1,4,6,7,8). *References*: (1) Abbott et al. 1986; (2) Howarth & Schmutz 1992; (3) Crowther 2007; (4) Hamann et al. 2006; (5) Crowther & Bohannan 1997; (6) Ignace et al. 2001; (7) Ignace et al. 2003b; (8) St.-Louis et al. 2009; (9) Gosset et al. 2005.